이학박사학위논문

Dynamic Scaling for Synchronization of Coupled Oscillators

결합된 진동자들의 동기화에 대한 동적 축척 이론

2013년 8월

서울대학교 대학원
물리·천문학부
최 철 호

Dynamic Scaling for Synchronization of Coupled Oscillators

Chulho Choi

Supervised by

Professor **Byungnam Kahng**

A dissertation submitted in partial fulfillment of
the requirements for the degree of
Doctor of Philosophy (Physics)

August 2013

Department of Physics and Astronomy
Graduate School
Seoul National University

Abstract

Dynamic Scaling for Synchronization of Coupled Oscillators

Chulho Choi
Department of Physics and Astronomy
Graduate School
Seoul National University

Systems with many elements interacting with each other often show collective behaviors. Synchronization is a typical example of the collective behaviors. At initial time, phases are different from each other because of the unique characteristics of each element (oscillator). As time goes on, interacting with others strongly, the oscillators adjust their phases and finally set the phases to almost mean phase of their neighbors.

The Kuramoto model is a simple and representative model for synchronization of coupled oscillators. For past decades many studies on the Kuramoto model has discovered much interesting results on synchronization of coupled oscillators. In the introduction, a little amount of these results of the previous studies on the Kuramoto model is introduced.

This dissertation has two main studies related to synchronization. The first part is a study on dynamic scaling for the Kuramoto model. Until now,

most of the previous studies has focused on the steady states. We also focus on temporal behavior of order parameter before the system goes to the steady state. We found that the order parameter of Kuramoto model evolves following a power-law of t at critical coupling strength K_c and conjectured dynamic scaling form of the Kuramoto model at the criticality. With several system sizes, we show that the r *v.s.* t graphs collapse into one single curve by using this scaling relation. And furthermore, the scaling exponents are explained by already-known exponents from finite-size scaling. All-to-all network, n-dimensional square lattices, classical random (Erdös-Rényi, ER) networks and scale-free (SF) networks are tested with natural frequencies chosen from Gaussian distribution. We also found that how to generate the natural frequencies from Gaussian distribution also affects temporal behaviors of the order parameter. In chapter 2, the finite-size scaling theory is described and confirmed numerically that is a base of dynamic scaling relation. And in chapter 3, we study dynamic scaling extensively.

The existence of dynamic scaling relation at critical point is an end in itself, and besides there is another reason why it is important practically. One may want to measure order parameter for very long simulation time to find a critical coupling strength with large system size N. But considering the computational cost of numerical integration for Kuramoto dynamics, there is always a practical limit of system size N or allowed simulation time. Thanks to the knowledge of dynamic scaling relation, one can find K_c in short simulation time even though the system does not enter to the steady state yet. The power-law behavior of order parameter distinguishes K_c very well and catches K_c clearly with a resolution of $(K - K_c)/K_c \sim \mathcal{O}(10^{-3})$.

The second part of this dissertation is a kind of application of Ku-

ramoto model to clustering problems and chapter 4 treats it. Clustering is to find modular structures of complex networks. We modify the Kuramoto model by introducing an additional term depending on the link betweenness centrality (BC) in interaction function. The additional term induces phase difference ($\in [0, \pi]$) between connected two oscillators as the BC on the link connecting them increases from the minimum to the maximum in the network. When this modified Kuramoto model is applied to networks with modular structure, the model drives each module to ordered state (phase synchronization), however the entire system remains in disordered state. Based on this phenomenon, we proposed a new clustering algorithm that shows quite good performance similar to other clustering algorithms and needs relatively little computational cost compared to other synchronization-based algorithms.

Finally, chapter 5 is devoted to the conclusion of this study. And some information which is helpful to simulate the Kuramoto model is in Appendices.

Keywords: Synchronization, Kuramoto model, Phase transition, Critical phenomena, Phase synchronization, Frequency synchronization, Dynamic scaling, Kuramoto model with inertia, Phase-locked state, Hysteresis, Coupled oscillators, Nonlinear dynamics, Complex network, Finite-size scaling, Critical slowing down, Clustering, Modular structure

Student Number: 2006-22912

Contents

List of figures

List of tables

Chapter 1

Introduction to Synchronization and Kuramoto Model

1.1 What is synchronization?

The definition of *syn·chronous* is "happening, existing, or arising at precisely the same time"(from Merriam-Webster dictionary). The prefix *syn-* means "at the same time"and *chronous*(from ancient Greek $\chi\rho\acute{o}\nu o\varsigma$) means "time". The definition of *synchronization* is "the state of being synchronous".

The more scientific definition of *synchronization* is provided by Stefano Boccaletti in his book [1]: "a general process wherein two (or many) dynamical systems (either equivalent or nonequivalent) are coupled or forced (periodically or noisy), in order to realize a collective or *synchrous* behavior".

Synchronization is a ubiquitous phenomenon in nature. In the 17th century Christiaan Huygens found that two pendulums hanging from the same ceiling of ship swing around to opposite direction to each other. He called it 'an odd kind of sympathy' [2]. Fireflies (some species in Asia and Africa) flash synchronously as they get into the rhythm [3]. Clapping timing of crowd gets the beat as time goes on. AC electric power generators in a same power grid adjust their frequencies spontaneously [4]. Cardiac pacemaker cells are also synchronized each other and control the contraction of heart muscles.

The reasons of these phenomena are not just coincidence but the in-

teractions between the members. The elements of the system interact with each other through some kinds of communication methods. A positive interaction may overcome the individual's characteristics to make one united characteristic of the whole system.

1.2 Coupled oscillators

Systems with many elements interacting with each other often show collective behaviors. Synchronization is a typical example of the collective behaviors. At $t = 0$ each element (oscillator) with its own unique characteristic has a phase different from others. As each element interacts with others it adjusts the phase and finally sets the phase to almost mean phase of its neighbors. We call this phenomenon phase synchronization. There are some models that consider amplitudes of oscillators as well as phases. Examples include Landau-Stuart limit cycle oscillator [5]. The model shows very interesting phenomena such as amplitude death [6]. We, however, do not treat this model in this thesis. We only focus on the phases of oscillators and assume that the amplitudes of oscillators are all same to 1 from now on.

Concerning synchronization of coupled oscillators, two kinds of synchronizations can be considered: frequency synchronization and phase synchronization.

Frequency synchronization refers to the state in which all oscillator's frequency (angular velocities) are same each other, so that oscillators evolve keeping their phase differences between neighbors. It may be called 'phase-locked state'.

Phase synchronization needs more strong condition. The oscillators should

have same phases as well as same frequencies.

1.3 Kuramoto model

Kuramoto model (KM) is a simple and representative model for synchronization of coupled oscillators [7–9]. (For easy introduction and historical view see [10], and see a review paper [11] for more information about KM and its variants.)

This model describes the dynamics of globally coupled oscillators as

$$\dot{\phi}_i(t) = \omega_i + \frac{K}{N}\sum_{j=1}^{N}\sin\left(\phi_j(t) - \phi_i(t)\right). \tag{1.1}$$

Here, ϕ is a phase and $\dot{\phi}$ is a phase velocity. The subscript (i or j) is an index for oscillators. ω is a natural frequency(angular velocity) which is oscillator's unique characteristic. Without any interactions the phase moves with this constant angular velocity. K is a coupling strength representing how strongly the oscillators interact with each other to take after its neighbors. N is the number of oscillators. ϕ and $\dot{\phi}$ are, of course, functions of time whereas ω, K and N are constant in this model. $\{\omega\}$ follows a certain distribution, $g(\omega)$. In general, the Gaussian distribution, $g(\omega) = \frac{1}{\sqrt{2\pi\sigma^2}}e^{-\frac{(\omega-\omega_0)^2}{2\sigma^2}}$ is often used. It has good properties making it easy to analyze mathematically: unimodal shape of distribution and perfect bilateral symmetry centered at mean value, ω_0. For given system size N and $g(\omega)$ the only control parameter remained is K. The system is synchronized when K is large enough to overcome the scattered $\{\omega\}$'s effect that inhibits the system from being synchronized. K value at which the transition from incoherent state to coherent (synchronized) state occurs is K_c and it is well known that

$K_c = \frac{2}{\pi g(\omega_0)}$, which leads to $K_c = \sqrt{8/\pi} \approx 1.595769$ with unit variance[8].

Eq. 1.1 can be generalized for complex networks as

$$\dot{\phi}_i(t) = \omega_i + \frac{K}{k_i} \sum_{j=1}^{N} A_{ij} \sin\Big(\phi_j(t) - \phi_i(t)\Big), \tag{1.2}$$

where k_i is a degree of ith node. Another extension is

$$\dot{\phi}_i(t) = \omega_i + K \sum_{j=1}^{N} A_{ij} \sin\Big(\phi_j(t) - \phi_i(t)\Big), \tag{1.3}$$

which is used in [12].

More generally it can be extended [13] as below:

$$\dot{\phi}_i(t) = \omega_i + \frac{K}{{k_i}^{1-\alpha}} \sum_{j=1}^{N} A_{ij} \sin\Big(\phi_j(t) - \phi_i(t)\Big). \tag{1.4}$$

Then, $\alpha = 0$ case returns to Eq. (1.2) and $\alpha = 1$ returns to Eq. (1.3).

1.4 Natural frequency

The sequence of natural frequencies $\{\omega\}$ is constant. Therefore, they are considered as quenched disorders. A distribution of quenched disorders plays an important role in determining the phase transition type. Here, we introduce a few distributions of the natural frequencies used frequently.

1.4.1 Gaussian distribution

Gaussian distribution is

$$g(\omega) = \frac{1}{\sqrt{2\pi\sigma^2}} e^{-\frac{(\omega-\omega_0)^2}{2\sigma^2}}. \tag{1.5}$$

In case of $m = 0$(the original Kuramoto model), it is known that if $g(\omega)$, probability density function of ω is unimodal and symmetric, the K_c is $\frac{2}{\pi g(\omega_0)}$. (For derivation of the formula see Eq. (2.39).) If we set $\omega_0 = 0$(or we are on the rotational frame of which angular velocity is ω_0) and $\sigma = 1$, we obtain $K_c = \sqrt{\frac{8}{\pi}} \approx 1.595769122$.

1.4.2 Cauchy distribution

Cauchy distribution is

$$g(\omega) = \frac{1}{\pi} \cdot \frac{\gamma}{(\omega - \omega_0)^2 + \gamma^2}. \tag{1.6}$$

In case of $m = 0$(the original Kuramoto model), choosing $\gamma = 1$ and $\omega_0 = 0$ gives $K_c = 2.0$.

1.4.3 Uniform distribution

$$g(\omega) = \begin{cases} \frac{1}{2\gamma} & \text{if } |\omega| \leq \gamma, \\ 0 & \text{otherwise} \end{cases} \tag{1.7}$$

It is known that the Kuramoto model with uniform distribution exhibits a first-order phase transition with $K_c = \frac{2}{\pi g(0)} = \frac{4\gamma}{\pi}$, $r_c = \frac{\gamma}{K_c} = \frac{\pi}{4}$ [14].

1.4.4 Double delta peaks

$$g(\omega) = \frac{1}{2}[\delta(\omega + \omega_0) + \delta(\omega - \omega_0)] \tag{1.8}$$

For $\omega_0 > T$, where T is thermal noise strength(effective temperature), it is known that $K_c = 4T$ [15], [16]. The Kuramoto model with noise is introduced in subsection 1.8.1.

Table 1.1: Symbols for distribution types.

Symbol	Distribution
GSS	Gaussian dist.
GSR	Gaussian-regular dist.
CCH	Cauchy dist.
CCR	Cauchy-regular dist.
UNF	uniform dist.
UNR	uniform-regular dist.
DDP	double delta peaks
DDR	double delta peaks-regular dist.

1.5 Sampling of natural frequency

How to generate the sequence of natural frequencies is an important issue. There are two kinds of sampling method: random sampling and regular sampling.

1.5.1 Random sampling

The sequence of natural frequencies, $\{\omega\}$ can be generated randomly from pdf $g(\omega)$ using random number generators. Usually, 64bit Mersenne Twister algorithm [17] gives random numbers of sufficiently good qualities.

1.5.2 Regular sampling

- Gaussian distribution: Regular sampling

  We can remove the frequency-disorder fluctuation in natural frequency by assigning the frequency of jth oscillator using

$$\int_{-\infty}^{\omega_j} g(\omega)\mathrm{d}\omega = \frac{-0.5+j}{N}, \quad j = 1, 2, \cdots, N. \tag{1.9}$$

([18]) and we call it XXX-regular distribution, XXX is a name of original distribution. By inserting Eq. (1.5) with $\omega_0 = 0$ into Eq. (1.9) we can obtain Gaussian-regular distribution,

$$\omega_j = \sqrt{2\sigma^2}\mathrm{erf}^{-1}\left(-1+\frac{2j-1}{N}\right), \quad j=1,2,\cdots,N. \tag{1.10}$$

- Cauchy distribution: Regular sampling

  Considering Eq. (1.9), one can obtain Cauchy-regular distribution using

  $$\omega_j = \gamma\tan\left(\frac{\pi}{2}(-1+\frac{2j-1}{N})\right), \quad j=1,2,\cdots,N. \tag{1.11}$$

  The authors of [19] used

  $$\omega_j = \gamma\tan\left(\frac{\pi}{2}(-1+\frac{2j}{N+1})\right), \quad j=1,2,\cdots,N, \tag{1.12}$$

  instead of Eq. (1.11). We use Eq. (1.11) for consistency with Eq. (1.9).

- Uniform distribution: Regular sampling

  This is how to allocate N numbers in range $[-\gamma,\gamma]$ uniformly (even-spaced).

  $$\omega_j = \gamma\left(-1+\frac{2j-1}{N}\right), \quad j=1,2,\cdots,N. \tag{1.13}$$

  Eq. (1.13) does not contain the boundaries, $\omega = \pm\gamma$. If the boundary values are contained, the equation is like below.

  $$\omega_j = \gamma\left(-1+\frac{2(j-1)}{N-1}\right), \quad j=1,2,\cdots,N. \tag{1.14}$$

  In $N\to\infty$ limit, both Eq. (1.13) and Eq. (1.14) go to uniform distribution. See D. Pazó's paper[14] for the issue induced from the differ-

ence of two distributions. Here, we use Eq. (1.13) for regular sampling for uniform distribution.

- Double delta peaks: Regular sampling

  Regular sampling of double delta peaks is very simple as

$$\omega_j = (-1)^j \omega_0, \quad j = 1, 2, \cdots, N. \tag{1.15}$$

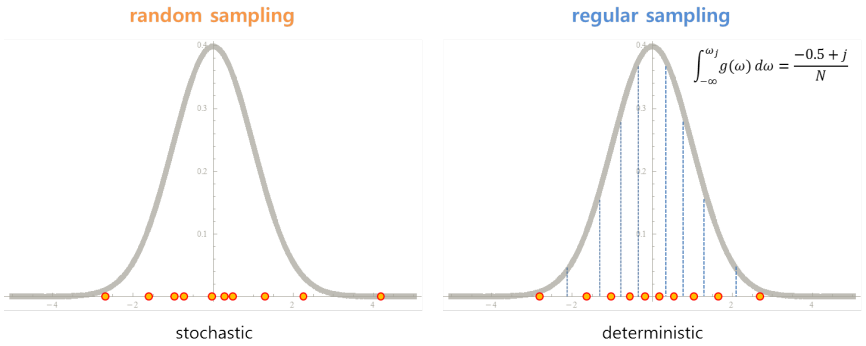

Figure 1.1: Two kinds of sampling methods for natural frequency: random sampling and regular sampling.

Table 1.2: Probability density functions and their regular sampling for several kinds of natural frequency distributions.

Distribution	PDF $g(\omega)$	Regular sampling ω_j
Gaussian	$\frac{1}{\sqrt{2\pi\sigma^2}} e^{-\frac{(\omega-\omega_0)^2}{2\sigma^2}}$	$\sqrt{2\sigma^2}\mathrm{erf}^{-1}\left(-1+\frac{2j-1}{N}\right)$
Cauchy	$\frac{1}{\pi}\cdot\frac{\gamma}{(\omega-\omega_0)^2+\gamma^2}$	$\gamma\tan\left(\frac{\pi}{2}(-1+\frac{2j-1}{N})\right)$
uniform	$\frac{1}{2\gamma}[1-\Theta(\lvert\omega\rvert-\gamma)]$ [1]	$\gamma\left(-1+\frac{2j-1}{N}\right)$
double delta peaks	$\frac{1}{2}[\delta(\omega+\omega_0)+\delta(\omega-\omega_0)]$	$(-1)^j\omega_0$

1.6 Measurement

In this section, some observable quantities are introduced.

1.6.1 Complex order parameter

Order parameter, r represents how strongly the oscillators are synchronized.

Complex order parameter is defined as

$$r(t)e^{i\psi(t)} \equiv \frac{1}{N}\sum_{j=1}^{N} e^{i\phi_j(t)}. \tag{1.16}$$

This quantity can be considered as a centroid of all phases in complex plane.

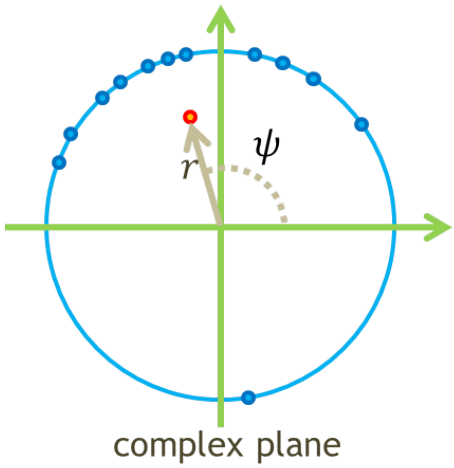

Figure 1.2: Complex order parameter as a centroid of all phases presented on complex plane.

We measure averaged order parameter,

$$R \equiv [\langle r \rangle], \tag{1.17}$$

where $[\cdots]$ means the ensemble average and $\langle \cdots \rangle$ means the time average.

Usually one collects the values of $r(t)$ after the system goes to the steady state, and takes their time averaged value $\langle r \rangle$. And the average for initial configurations ($\phi_i(0)$ and $\{\omega_i\}$) also can be considered as $[\langle r \rangle]$.

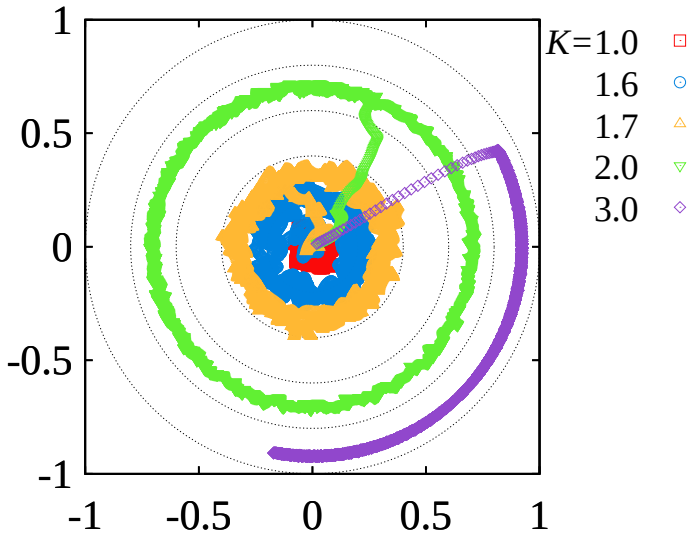

Figure 1.3: Complex order parameter, $r(t)$ are plotted for several K values in complex plane. Here $t = 0, 0.1, 0.2, \cdots, 500$. The system size, $N = 1600$.

The order parameter can be understood by its relation with the width of interface. In surface growth problem, the width of interface is defined as

$$w(L,t) \equiv \sqrt{\frac{1}{L}\sum_{i=1}^{L}\left(h(i,t) - \bar{h}(t)\right)^2}, \tag{1.18}$$

where L is a lattice size, h is height, $\bar{h}$ is mean height and i is index for site. For random deposit (RD) model which has no correlation of interface, it is well-known that $w \sim t^{\beta'=1/2}$. (See chapter 4 in the book [20] for more information about RD model.) Here β' is the growth exponent. We use primed character β' to distinguish it from β used in $r \sim \epsilon^{\beta}$. The authors of

[21] considered the relation between order parameter r and interface width w as

$$r \sim \exp\Big(-\frac{w^2}{2}\Big) \tag{1.19}$$

in the stationary state.

1.6.2 Susceptibility, χ

Let $[\cdots]$ denote configuration average(ensemble average) and $\langle\cdots\rangle$ time average in the steady state. Then the order of two kinds of averages makes several definitions of susceptibility as in definitions of Binder's cumulant [22].

$$\chi^{(1)} \equiv N[\langle r^2\rangle - \langle r\rangle^2] = N\Big([\langle r^2\rangle] - [\langle r\rangle^2]\Big). \tag{1.20}$$

is an average over χ_i which is susceptibility of ith ensemble.

$$\chi^{(2)} \equiv N\Big([\langle r^2\rangle] - [\langle r\rangle]^2\Big). \tag{1.21}$$

is susceptibility calculated with $r_i((N_{\text{skip}}+j)\mathrm{d}t)$ data for $i = 1, \cdots, N_{\text{ens}}$ and $j = 1, \cdots, N_{\text{take}}$. N_{skip} is the number of discarded data points and N_{take} is the number of taken data points used to calculate average value.

$$\chi^{(3)} \equiv N\Big([\langle r\rangle^2] - [\langle r\rangle]^2\Big). \tag{1.22}$$

is susceptibility of $\langle r\rangle$.

These three kinds of definitions for χ are related to each other as

$$\chi^{(2)} = \chi^{(1)} + \chi^{(3)}. \tag{1.23}$$

1.6.3 Standard deviation, σ

$$\sigma^{(1)} \equiv \sqrt{[\langle r^2\rangle - \langle r\rangle^2]} = \sqrt{[\langle r^2\rangle] - [\langle r\rangle^2]}. \tag{1.24}$$

$$\sigma^{(2)} \equiv \sqrt{[\langle r^2\rangle] - [\langle r\rangle]^2}. \tag{1.25}$$

$$\sigma^{(3)} \equiv \sqrt{[\langle r\rangle^2] - [\langle r\rangle]^2}. \tag{1.26}$$

Note that $[\langle r^2\rangle] \geq [\langle r\rangle^2] \geq [\langle r\rangle]^2$ always. Therefore $\sigma^{(2)} \geq \sigma^{(1)}$ and $\sigma^{(2)} \geq \sigma^{(3)}$. These three kinds of standard deviations are related as

$$\left(\sigma^{(2)}\right)^2 = \left(\sigma^{(1)}\right)^2 + \left(\sigma^{(3)}\right)^2. \tag{1.27}$$

1.6.4 Binder's cumulant, U_4

Binder's cumulant is defined as $U_4 \equiv 1 - \frac{\overline{r^4}}{3\overline{r^2}^2}$, where $\overline{\cdots}$ is any kinds of averaging [23], [24]. We have two kinds of averaging, ensemble average $[\cdots]$ and time average $\langle\cdots\rangle$. The order of two kinds of averaging makes several definitions of Binder's cumulant.

$$U_4^{(1)} \equiv \left[1 - \frac{\langle r^4\rangle}{3\langle r^2\rangle^2}\right] = 1 - \left[\frac{\langle r^4\rangle}{3\langle r^2\rangle^2}\right] \tag{1.28}$$

is an average of each ensemble's U_4.

$$U_4^{(2)} \equiv 1 - \frac{[\langle r^4\rangle]}{3[\langle r^2\rangle]^2} \tag{1.29}$$

is calculated by all data points from every ensemble and every time.

$$U_4^{(3)} \equiv 1 - \frac{[\langle r\rangle^4]}{3[\langle r\rangle^2]^2} \tag{1.30}$$

is Binder's cumulant of $\langle r \rangle$.

Note that the name of U_4 is different from [22]. Other definitions for Binder's cumulant are also possible mathematically but we think they do not have any physical meaning.

1.7 Phase transition

In the Kuramoto model, natural frequencies $\{\omega_i\}$ disperse the oscillators. Without coupling term (in the limit of $K/\sigma \to 0$), therefore, the oscillators may have random constant speed. Hence the order parameter is nearly zero, $r \sim N^{-1/2}$. We call this state *disordered state*. In the opposite limit of $K/\sigma \gg 1$, the oscillates synchronize their phases with each other. The order parameter is nearly one. This state is called *ordered state*.

Considering magnetic systems as Ising model, we can consider the coupling strength K as a inverse temperature. The absolute value of magnetization (order parameter) per site is nearly zero when temperature $T \to \infty$ and nearly one when $T \to 0$. A phase transition in synchronization has been an interesting subject as in the magnetization systems. At critical coupling strength K_c, the systems exhibits a phase transition from disordered state ($K < K_\mathrm{c}$) to ordered state ($K > K_\mathrm{c}$).

It is well known that the Kuramoto model with natural frequencies following Gaussian distribution exhibits a *continuous phase transition*. Gaussian-like distributions - unimodal and bilateral symmetric distributions - make a continuous phase transition at $K = K_\mathrm{c} = \frac{2}{\pi g(\omega=0)}$.

On the other hand, bimodal distributions make a *first-order phase transition*. And as a boundary case between unimodality and bimodality, the

uniform distribution makes a first-order phase transition [14].

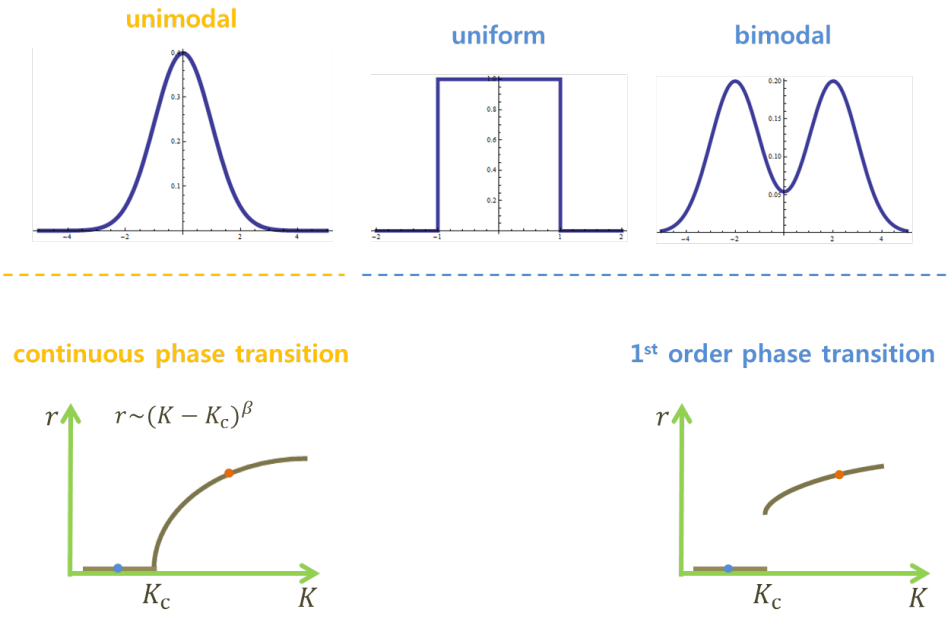

Figure 1.4: Relation between natural frequency distributions and phase transition types.

1.8 Variants of Kuramoto model

1.8.1 Kuramoto model with random noise

Systems in nature might be affected by some kinds of noises. In this sense, Kuramoto model with external random noise is a more natural model than the original Kuramoto model. The authors of [25] considered Gaussian white noise η as

$$\dot{\phi}_i(t) = \omega_i + \frac{K}{N}\sum_{j=1}^{N}\sin\left(\phi_j(t) - \phi_i(t)\right) + \eta_i(t). \tag{1.31}$$

The Gaussian white noise is characterized by $\langle \eta_i(t) \rangle = 0$ and $\langle \eta_i(t)\eta_j(t') \rangle = 2T\delta_{ij}\delta(t-t')$. In other words, $\eta_i(t)$ is a random number chosen from Gaus-

sian distribution with variance $2T$. T is called *effective temperature* and changes the critical coupling strength as

$$K_{\mathrm{c}}(T) = 2 \Big/ \int_{-\infty}^{\infty} \frac{T}{T^2+\omega^2} g(\omega) \mathrm{d}\omega. \tag{1.32}$$

1.8.2 Kuramoto model with periodic driving force

Kuramoto model with periodic driving force was studied in [26]. The dynamics of oscillators is governed by

$$\dot{\phi}_i(t) = \omega_i + \frac{K}{N} \sum_{j=1}^{N} \sin\left(\phi_j(t) - \phi_i(t)\right) + I_i \cos \Omega t, \tag{1.33}$$

where I_i is the periodic driving strength and Ω is the frequency of the driving. The authors of [26] found that uniform distribution as $g(\omega)$ and double delta function as $f(I)$ induce periodic synchronization.

1.8.3 Kuramoto model with inertia

Kuramoto model with inertia term was proposed by [19, 27]. Dynamics of oscillators with inertia is described as

$$m\ddot{\phi}_i(t) + \dot{\phi}_i(t) = \omega_i + \frac{K}{N} \sum_{j=1}^{N} \sin\left(\phi_j(t) - \phi_i(t)\right), \tag{1.34}$$

where m is inertia of each oscillators. Eq. (1.34) can be understood as equations of motion of oscillators with inertia ($m\ddot{\phi}$) influenced by damping ($\dot{\phi}$) and external driving force (ω). Note that these equations are not on velocities but on forces. It was found that a first-order phase transition occurs for finite large inertia. The evidence of the discontinuous phase transition

is a hysteresis curve in (r, K) plane. In this case the drifting oscillators contribute to order parameter as well as the rocked oscillators. The existence of nonzero critical inertia, m_c above which the system exhibits a first-order phase transition had remained as an open problem. This puzzle was solved by [28].

1.8.4 Kuramoto model with inertia and external periodic force

The authors of [28] studied Kuramoto model with inertia and external periodic force. The equations of motion are

$$m\ddot{\phi}_i(t) + \dot{\phi}_i(t) = \omega_i + \frac{K}{N}\sum_{j=1}^{N}\sin\left(\phi_j(t) - \phi_i(t)\right) + I_i\cos\Omega t, \tag{1.35}$$

where I_i and Ω have same meanings as defined in Eq. (1.33). Clearly, $I = 0$ case corresponds to Eq. (1.34). Any nonzero inertia make the system exhibit a first-order phase transition. r_c, the order parameter at $K = K_c$ is a function of inertia. Considering a leading term, It is proportional to inertia in $m \to 0$ limit. This is the reason why the numerical confirmation was so difficult for small inertia values. $I \neq 0$ case also gives periodic synchronization.

1.8.5 Kuramoto model with inertia and random noise

The authors of [16] studied on Kuramoto model with inertia and random noise. The dynamics is governed by

$$m\ddot{\phi}_i(t) + \dot{\phi}_i(t) = \omega_i + \frac{K}{N}\sum_{j=1}^{N}\sin\left(\phi_j(t) - \phi_i(t)\right) + \eta_i(t). \tag{1.36}$$

They used Cauchy distribution Eq. (1.6) as natural frequency's distribution and found that the critical coupling strength in the small noise limit ($T \ll 1$):

$$K_{\mathrm{c}} = 2\gamma(m\gamma + 1) + \frac{2(2+3m\gamma)}{2+m\gamma}T + O(T^2) \tag{1.37}$$

for $m = O(1)$, and

$$K_{\mathrm{c}} = 2\gamma(m\gamma + 3) + \frac{4}{m} \tag{1.38}$$

for $mT = 1$.

1.8.6 Kuramoto model on complex networks

- n-dimensional square lattice

  Kuramoto model on n-dimensional square lattices was studied in [29], [21], [30]. The governing dynamics equation is Eq. (1.3). The lower critical dimension, d_l^P is 4, which means that no phase synchronization occurs up to $d = 4$ in the thermodynamic limit ($N \to \infty$), or phase synchronization is possible only for $d \geq 5$. They found relation between order parameter and surface fluctuation growth width as $r = \exp(-W^2/2)$.

- Erdős Rényi(ER) network and scale-free(SF) network

  The difference of clustering processes on ER networks and SF networks was studied by [12], [31]. (See [32] for more detailed information about complex networks(ER and SF networks).) They investigated how synchronized clusters grow as coupling strength increases using uniform distribution of natural frequencies. For ER network, several small clusters - each clusters has similar sizes - are formed with

small K. As K increases, these small clusters are merged into some larger clusters. And every clusters form one large cluster with large K at last. For SF network, on the other hand, a giant cluster absorbs smaller neighboring clusters and grows gradually as K increases.

- scale-free (SF) network and degree-correlated natural frequency

  The authors of [33] found that degree-correlated natural frequency as $\omega_i = k_i$ induces a first-order phase transition on SF network transition. And [34] calculated the critical coupling strength using mean field approaching as

  $$K_{\mathrm{c}} = \frac{2}{\pi \langle k \rangle P(\langle k \rangle)}, \tag{1.39}$$

  where $P(k)$ is a distribution function of degrees and $\langle k \rangle$ is mean degree. Later [35] discovered that SF network with $2 < \gamma < 3$ (γ is a degree exponent of SF network.) only exhibits a first-order phase transition and SF network with $\gamma > 3$ undergoes a continuous phase transition. Especially $\gamma = 3$ case has properties of both first-order and second-order phase transition. It shows an abrupt emergence of synchronization and a critical singularity. They call it hybrid phase transition.

Table 1.3: Studies on Kuramoto model and its variants.

Network	$g(\omega)$	Inertia m	Noise ξ	Driving I	Delay τ	Ref.	Phase Transition	Etc.
FCN	GSS	-	-	-	-	[8]	2nd	-
FCN	GSS-like	-	-	o	-	[26]	2nd or 1st	-
FCN	CCH(GSS)	o(large)	-	-	-	[19]	1st	-
FCN	GSS-like	o(small)	-	o	-	[28]	1st	-
FCN	GSS-like	o	o	-	-	[36], [37]	2nd for $T \gg 0$	-
FCN	CCH	o	o	-	-	[16]		-
FCN	GSS	o	-	-	o	[38]		-
FCN	adaptive	△	-	-	△	[39]		adaptive ω, include m or τ
LTC	GSS	-	-	-	-	[29], [21], [30]	2nd	
SF	UNF	-	-	-	-	[40], [41]	2nd	-
SF	DEG	-	-	-	-	[33], [34], [35]	1st for $2 < \gamma < 3$, 2nd for $\gamma \geq 3$	-
SF	GSS	-	-	-	-	[42]	2nd	-
SF, ER	UNF	-	-	-	-	[12], [31]	2nd	cluster development
SF, ER	SDP	-	o(uniform)	-	-	[43]	2nd for SF($\gamma = 3$), 1st-like for ER	$\exists W_c$ for noise

1.9 Summary

Synchronization is a ubiquitous phenomenon in nature. A great deal of attention, therefore, has been attracted to study models for synchronization phenomenon. We introduced Kuramoto model which is a representative synchronization model and some of variations on it. Kuramoto model is a model for system which is composed of globally coupled phase oscillators. As the coupling strength varies, the system exhibits a phase transition at the critical coupling strength. The type of phase transition is determined by the shape of natural frequency's distribution function. Unimodal and symmetric distributions such as Gaussian form induce a second-order phase transition, whereas Bimodal shapes lead to a first-order phase transition. We defined some measurable quantities - order parameter, susceptibility, standard deviation and Binder's cumulant - that are major characteristics of systems.

Chapter 2

Finite-Size Scaling

Before the system gets into the steady state, order parameter, r increases or decreases toward its saturation value $r_{\rm sat}$ from initial value, r_0. For a given coupling strength K, $r_{\rm sat}$ depends on the system size, N. In the lower critical regime ($\epsilon \equiv (K - K_{\rm c})/K_{\rm c} \ll 0$), $r_{\rm sat} \sim N^{-1/2}$ because the randomness of natural frequencies dominates the dynamics. In the upper critical regime ($\epsilon \gg 0$), on the other hand, the coupling term is dominant compared to the randomness of natural frequencies. So $r_{\rm sat}$ has a finite non-zero value. At $\epsilon = 0$, the effect of coupling term is comparable to the randomness of natural frequencies, hence $r_{\rm sat}$ shows a critical power-law behavior as $r_{\rm sat} \sim N^{-\beta/\bar{\nu}}$.

2.1 Critical exponents

In this section, we introduce the *critical exponents* of synchronization problem that describe behaviors of the given system at and near critical point in *thermodynamic limit*. The term *thermodynamic limit* means a limit of infinite system size ($N \to \infty$).

Correlation length diverges at the critical point $K = K_{\rm c}$ as

$$\xi \sim \epsilon^{-\nu_\perp}, \tag{2.1}$$

where $\epsilon \equiv (K - K_{\rm c})/K_{\rm c}$ is a *reduced coupling strength*.

Correlation time diverges at the critical point $\epsilon = 0$ as

$$\tau \sim \epsilon^{-\nu_\parallel} \tag{2.2}$$

$$\sim \left(\xi^{-\frac{1}{\nu_\perp}}\right)^{-\nu_\parallel} = \xi^{\frac{\nu_\parallel}{\nu_\perp}} \equiv \xi^z. \tag{2.3}$$

Order parameter in steady state behaves at and above the critical point $\epsilon = 0$ as

$$r_{\text{sat}} \sim \epsilon^\beta. \tag{2.4}$$

Susceptibility in steady state diverges at the critical point $\epsilon = 0$ as

$$\chi \sim |\epsilon|^{-\gamma}. \tag{2.5}$$

2.2 Finite-size effect and scaling function

As mentioned in the previous section, the correlation length diverges at criticality in the thermodynamic limit. With finite number of oscillators, however, one should take into account the *finite-size effect*. The correlation length cannot exceed the system size $L = N^{\frac{1}{d}}$ even though $\epsilon \sim 0$. In other words, L is the maximum limit of the correlation length. (For all-to-all network, *correlation volume* is a more appropriate term than correlation length. In that case, N is the maximum limit of the correlation volume.) From Eq. (2.1), therefore, we obtain

$$\xi \sim \epsilon^{-\nu_\perp} \sim L = N^{\frac{1}{d}} \tag{2.6}$$

$$\rightarrow \quad \epsilon \sim N^{-\frac{1}{d\nu_\perp}} \equiv N^{-\frac{1}{\bar{\nu}}} \tag{2.7}$$

$$\therefore \quad \epsilon N^{\frac{1}{\bar{\nu}}} \sim \text{const} \tag{2.8}$$

near $\epsilon = 0$.

From Eq. (2.3) and Eq. (2.6), we obtain

$$\tau \quad \sim \quad \xi^z \sim N^{\frac{z}{d}} \equiv N^{\bar{z}}. \tag{2.9}$$

- order parameter

  From Eq. (2.4) and Eq. (2.7), we obtain

  $$r_{\text{sat}} \sim \epsilon^{\beta} \sim N^{-\frac{\beta}{\bar{\nu}}}. \tag{2.10}$$

  Eq. (2.10) can be written more generally as

  $$r_{\text{sat}} \sim N^{-\frac{\beta}{\bar{\nu}}} f_r(\epsilon N^{\frac{1}{\bar{\nu}}}), \tag{2.11}$$

  where $f_r(x)$ is a scaling function for the order parameter which behaves as $f_r(x) \sim x^{\beta}$ for $x \gg 1$, const for $x \to 0$. Then one can verify that Eq. (2.11) becomes $r_{\text{sat}} \sim N^{-\frac{\beta}{\bar{\nu}}}$ when $\epsilon = 0$ and $r_{\text{sat}} \sim \epsilon^{\beta}$ when $N \to \infty$.

- susceptibility

  Similarly, from Eq. (2.5) and Eq. (2.7), we get

  $$\chi \sim |\epsilon|^{-\gamma} \sim N^{\frac{\gamma}{\bar{\nu}}}. \tag{2.12}$$

  And Eq. (2.12) can be written more generally as

  $$\chi \sim N^{\frac{\gamma}{\bar{\nu}}} f_{\chi}(\epsilon N^{\frac{1}{\bar{\nu}}}), \tag{2.13}$$

  where $f_{\chi}(x)$ is a scaling function for susceptibility which behaves as

$f_\chi(x) \sim |x|^{-\gamma}$ for $x \gg 1$, const for $x \to 0$. Then one can verify that Eq. (2.13) becomes $\chi \sim N^{\frac{\gamma}{\bar{\nu}}}$ when $\epsilon = 0$ and $\chi \sim |\epsilon|^{-\gamma}$ when $N \to \infty$ again.

- standard deviation

  Scaling function for standard deviation is

$$\sigma \sim N^{\frac{\lambda}{\bar{\nu}}} f_\sigma(\epsilon N^{\frac{1}{\bar{\nu}}}). \tag{2.14}$$

  Because of $\sigma = \sqrt{\chi/N}$, we get $2\lambda/\bar{\nu} = \gamma/\bar{\nu} - 1$, or

$$\gamma = \bar{\nu} + 2\lambda. \tag{2.15}$$

- Binder's cumulant

  Scaling function for Binder's cumulant is

$$U_4 \sim f_{U_4}(\epsilon N^{\frac{1}{\bar{\nu}}}). \tag{2.16}$$

2.3 Numerical results of finite-size scaling

Eq. (2.11) and Eq. (2.13) are called *finite-size scaling*. In this section, we verify these scaling relations with numerical simulations. We used Gaussian distribution (Eq. (1.5)) as natural frequency distribution.

By inserting Eq. (1.16) to Eq. (1.1) we get

$$\dot{\phi}_i(t) = \omega_i + Kr(t)\sin\big(\theta(t) - \phi_i(t)\big). \tag{2.17}$$

We calculated $\phi_i(t)$ for all i numerically using Eq. (2.17). Every numerical result in this thesis is obtained by using 4th order Runge-Kutta (RK4)

method with dt=0.01 or 0.05. Without any specific mention, Gaussian distribution with unit variance ($\sigma = 1$) is used for natural frequencies. See Appendix A for more detailed description about the numerical simulation method.

2.3.1 Order parameter

The finite-size scaling form of the order parameter, Eq. (2.11) is confirmed in Fig. 2.1. The $r_{\rm sat}$ *vs.* K graphs for several system sizes are, of course, different from each other in the left of Fig. 2.1 but collapsed into one single curve in the right of Fig. 2.1 that are drawn using the finite-size scaling law.

Here we used $\beta = 1/2$ and $\bar{\nu} = 5/2$ which mean $\beta/\bar{\nu} = 1/5$. $\bar{\nu} = 5/2$ is obtained by considering the sample-to-sample fluctuation of natural frequencies in [30]. We confirmed $\beta/\bar{\nu} \approx 0.228$ numerically in the left panel of Fig. 2.2.

2.3.2 Susceptibility

When one measures susceptibility to obtain the exponent $\gamma/\bar{\nu}$ of Eq. (2.13), it can be performed in two different ways. To obtain $\gamma/\bar{\nu}$ one should make the scaling function constant and two ways are possible to do it. The first method is to measure susceptibility at $K = K_{\rm c} \equiv \lim_{N\to\infty} K_{\rm c}(N)$. Then f_χ is constant independent on system size N. The second method is to measure susceptibility at $K = K_{\rm c}(N)$. $K_{\rm c}(N)$ is a coupling strength at which the susceptibility has a maximum value for given N. Because $|K_{\rm c} - K_{\rm c}(N)| \sim N^{-\frac{1}{\bar{\nu}}}$, f_χ is independent on system size N again[44]. In the Kuramoto model we know that $K_{\rm c} = \frac{2}{\pi g(0)}$ exactly. So we used the first method to obtain $\gamma/\bar{\nu}$.

In Fig. 2.3, Fig. 2.4 and Fig. 2.5, three kinds of susceptibilities are

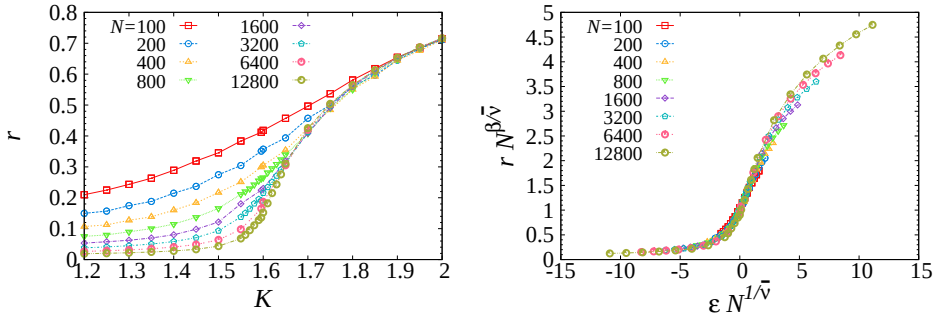

Figure 2.1: Finite-size scaling for order parameter: random sampling of $\{\omega_j\}$. (left) r *vs.* K with several Ns and (right) its finite-size scaling with known exponents $\beta = 1/2$ and $\bar{\nu} = 5/2$.

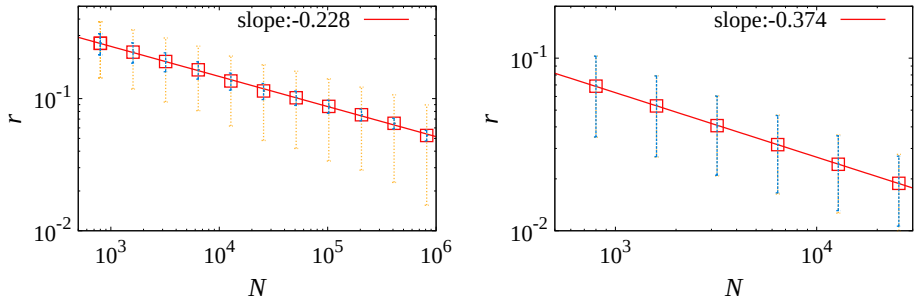

Figure 2.2: $r_{\rm sat}$ *vs.* N at the criticality for fully-connected network: The slope is $-\beta/\bar{\nu}$. The lengths of error bars are $\sigma^{(1)}$(blue) and $\sigma^{(2)}$(orange). $r(0) \sim N^{-1/2}$. (left) random sampling of $\{\omega_j\}$. $\beta/\bar{\nu} \approx 0.228$. The number of ensemble is 1000. (right) regular sampling of $\{\omega_j\}$. $\beta/\bar{\nu} \approx 0.374$. The number of ensemble is 500 for $N \leq 12800$, 200 for $N = 25600$.

plotted for various K. And we obtained $\gamma^{(1)}/\bar{\nu} \approx 1/3$ and $\gamma^{(2)}/\bar{\nu} \approx 2/3$ in a case of random sampling from numerical simulation in the left panel of Fig. 2.6. Considering $\bar{\nu} = 5/2$ [30], we get $\gamma^{(1)} \approx 5/6$ and $\gamma^{(2)} \approx 5/3$. These are different from the previous result $\gamma/\bar{\nu} = 1/2$ studied in [45], where supercritical finite-size scaling law and subcritical scaling law were predicted as $\sqrt{\chi} = N^{1/4}\Psi_+(N^2\epsilon)$ and $\sqrt{\chi} = N^{1/4}\Psi_-(N^{1/2}|\epsilon|)$, respectively. At that time the sample-to-sample fluctuation of natural frequencies was not considered, so the known value of $\bar{\nu}$ was not 5/2 but 2, which gives us $\gamma = 1$ in turn.

2.3.3 Standard deviation

We measured three kinds of standard deviations defined in Eq. (1.24), (1.25), (1.26) and plotted σ *vs.* N graphs in Fig. 2.7.

2.3.4 Binder's cumulant

We measured three kinds of Binder's cumulant defined in Eq. (1.28), (1.29), (1.30). U_4 *vs.* K graphs and their scaling functions (Eq. (2.16)) are drawn in Fig. 2.8, Fig. 2.9 and Fig. 2.10. U_4 *vs.* N graphs are drawn in Fig. 2.11

Table 2.1: Summary for exponents obtained from numerical simulation.

Exponent	Random sampling	Regular sampling
$\beta/\bar{\nu}$	0.228	$0.374 \approx 3/8$
$\gamma^{(1)}/\bar{\nu}$	$0.336 \approx 1/3$	0.184
$\gamma^{(2)}/\bar{\nu}$	$0.663 \approx 2/3$	0.224
$\gamma^{(3)}/\bar{\nu}$	0.686	1.086
$\lambda^{(1)}/\bar{\nu}$	$-0.332 \approx -1/3$	-0.408
$\lambda^{(2)}/\bar{\nu}$	$-0.169 \approx -1/6$	-0.388
$\lambda^{(3)}/\bar{\nu}$	-0.157	0.043

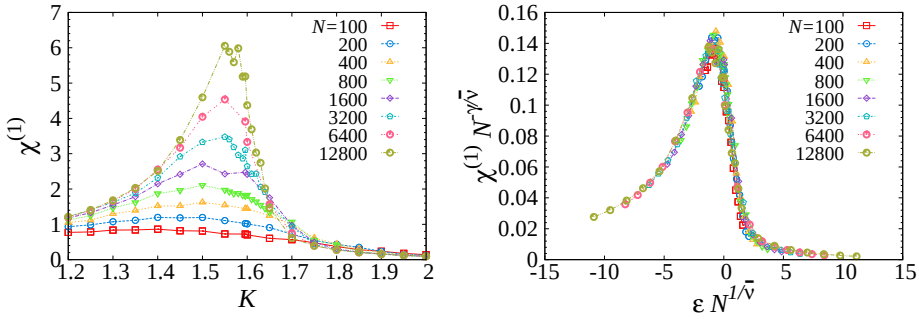

Figure 2.3: Finite-size scaling for susceptibility I: random sampling of $\{\omega_j\}$. (left) $\chi^{(1)}$ *vs.* K with several Ns and (right) its finite-size scaling with $\gamma^{(1)}/\bar{\nu} = 0.4$ and $\bar{\nu} = 5/2$. $\gamma^{(1)}/\bar{\nu} = 0.4$ is chosen for curves of different system sizes to collapse into a single curve. Simulations with larger system sizes, however, give a different value of $\gamma^{(1)}/\bar{\nu} (\approx 1/3)$ that is shown in Fig. 2.6.

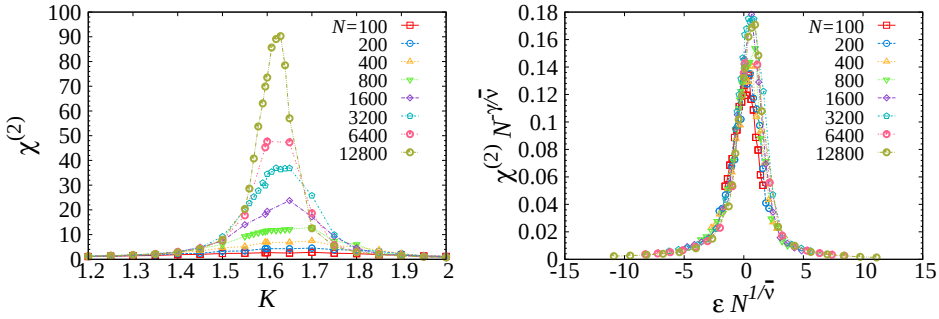

Figure 2.4: Finite-size scaling for susceptibility II: random sampling of $\{\omega_j\}$. (left) $\chi^{(2)}$ *vs.* K with several Ns and (right) its finite-size scaling with $\bar{\nu} = 5/2$ and $\gamma^{(2)}/\bar{\nu} = 0.663$ which is obtained from the slope of Fig. 2.6.

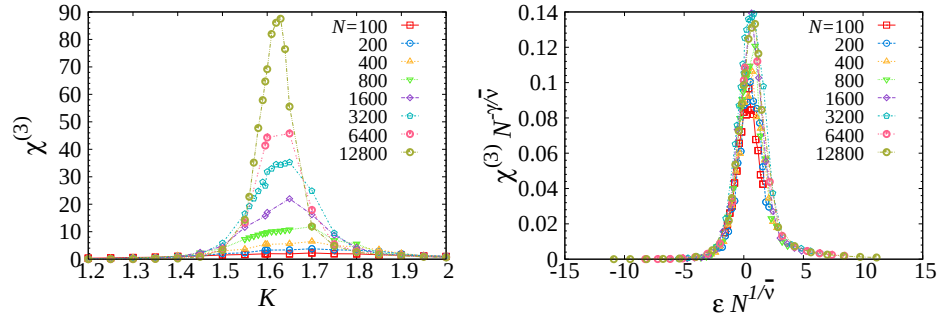

Figure 2.5: Finite-size scaling for susceptibility III: random sampling of $\{\omega_j\}$. (left) $\chi^{(3)}$ *vs.* K with several Ns and (right) its finite-size scaling with $\bar{\nu} = 5/2$ and $\gamma^{(3)}/\bar{\nu} = 0.686$ which is obtained from the slope of Fig. 2.6.

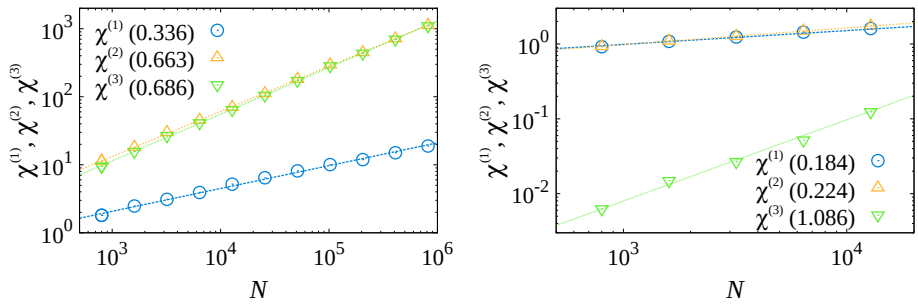

Figure 2.6: χ *vs.* N at the criticality for fully-connected network: The slope is $\gamma/\bar{\nu}$. $r(0) \sim N^{-1/2}$. (left) random sampling of $\{\omega_j\}$. $\gamma^{(1)}/\bar{\nu} \approx 0.336$. $\gamma^{(2)}/\bar{\nu} \approx 0.663$. $\gamma^{(3)}/\bar{\nu} \approx 0.686$. The number of ensemble is 1000. (right) regular sampling of $\{\omega_j\}$. $\gamma^{(1)}/\bar{\nu} \approx 0.184$. $\gamma^{(2)}/\bar{\nu} \approx 0.224$. $\gamma^{(3)}/\bar{\nu} \approx 1.086$. The number of ensemble is 500 for $N \leq 12800$, 200 for $N = 25600$.

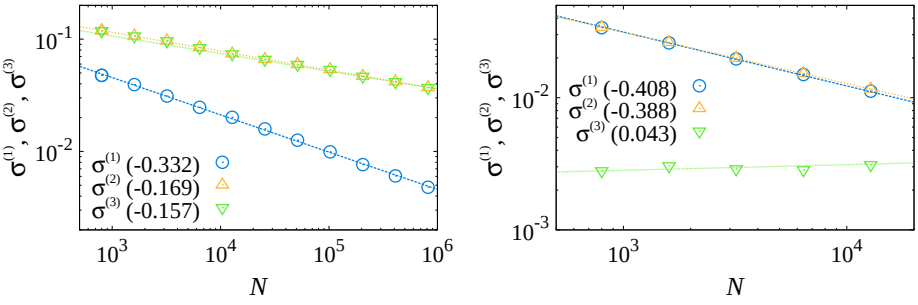

Figure 2.7: σ *vs.* N at the criticality for fully-connected network: The slope is $-\lambda/\bar{\nu}$. $r(0) \sim N^{-1/2}$. (left) random sampling of $\{\omega_j\}$. $\lambda^{(1)}/\bar{\nu} \approx 0.332$. $\lambda^{(2)}/\bar{\nu} \approx 0.169$. $\lambda^{(3)}/\bar{\nu} \approx 0.157$. The number of ensemble is 1000. (right) regular sampling of $\{\omega_j\}$. $\lambda^{(1)}/\bar{\nu} \approx 0.408$. $\lambda^{(2)}/\bar{\nu} \approx 0.388$. $\lambda^{(3)}/\bar{\nu} \approx 0.043$. The number of ensemble is 500 for $N \leq 12800$, 200 for $N = 25600$.

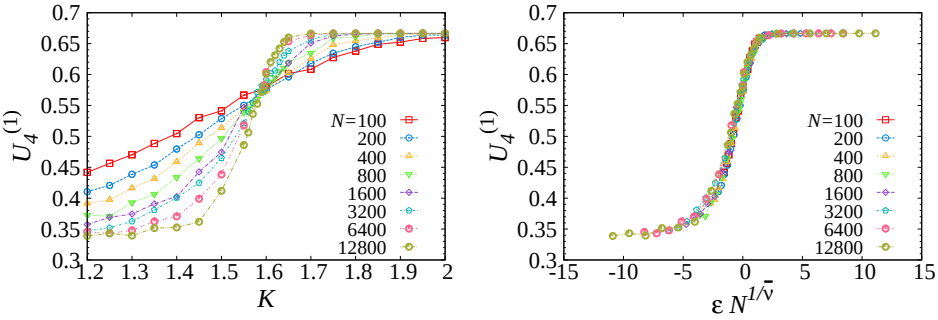

Figure 2.8: Ffinite-size scaling for Binder's cumulant I: random sampling of $\{\omega_j\}$. (left) $U_4^{(1)}$ *vs.* K with several Ns and (right) its finite-size scaling with $\bar{\nu} = 5/2$.

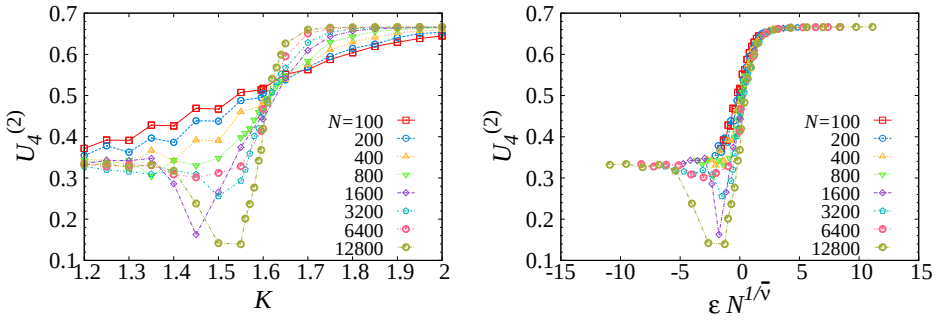

Figure 2.9: Finite-size scaling for Binder's cumulant II: random sampling of $\{\omega_j\}$. (left) $U_4^{(2)}$ *vs.* K with several Ns and (right) its finite-size scaling with $\bar{\nu} = 5/2$.

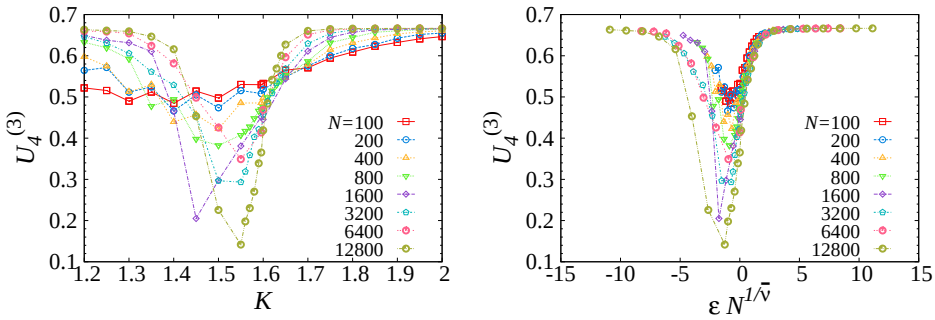

Figure 2.10: Finite-size scaling for Binder's cumulant III: random sampling of $\{\omega_j\}$. (left) $U_4^{(3)}$ *vs.* K with several Ns and (right) its finite-size scaling with $\bar{\nu} = 5/2$.

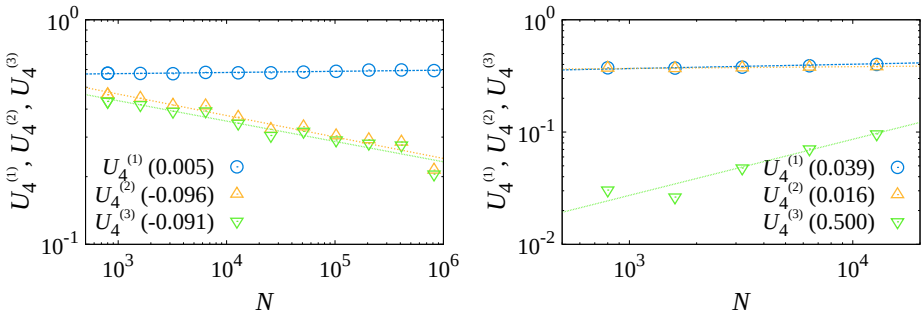

Figure 2.11: U_4 *vs.* N at the criticality for fully-connected network: The slope should be 0 because $U_4 \sim N^0$. $r(0) \sim N^{-1/2}$. (left) random sampling of $\{\omega_j\}$. The number of ensemble is 1000. (right) regular sampling of $\{\omega_j\}$. The number of ensemble is 500 for $N \leq 12800$, 200 for $N = 25600$.

2.3.5 Effect of frequency-disorder fluctuation

Frequency-disorder fluctuation affects to the thermodynamic exponent $\bar{\nu}$, but does not affect to β. The reason why β does not depend on the existence of frequency-disorder fluctuation is that the system should go to the same r *vs.* K curve in thermodynamic limit. But the intermediate pathways from $r(N)$ *vs.* K curve of finite-size to $r(\infty)$ *vs.* K curve are affected by the existence of frequency-disorder fluctuation.

We tested the self-averageness [22, 46–48] of order parameter. If a system is self-averageable, its Binder's cumulant $U_4^{(1)}$ should be almost similar to $U_4^{(2)}$. As shown in Fig. 2.11, the regular sampling case is self-averageable, whereas the random sampling case is not. The histograms of order parameters measured in a steady state support this argument in Fig. 2.12.

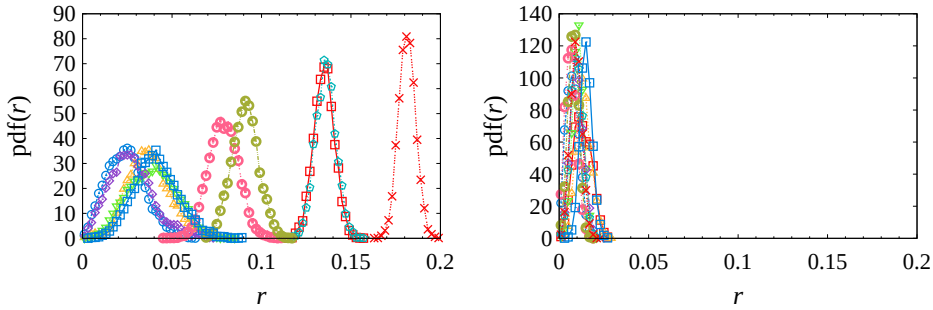

Figure 2.12: pdf(r) *vs.* r for fully-connected network: $r(0) \sim N^{-1/2}$. $K = K_c$. $N = 102400$. 10 ensembles are plotted. Each distribution of r was obtained from 10^5 data points in the steady state. (left) random sampling of $\{\omega_j\}$, (right) regular sampling of $\{\omega_j\}$.

2.4 Analytic approach: Self consistency equation of order parameter

As described before, Kuramoto model is a set of coupled differential equations:

$$\dot{\phi}_i = \omega_i + \frac{K}{N}\sum_{j=1}^{N}\sin(\phi_j - \phi_i). \tag{2.18}$$

And complex order parameter is defined as

$$r(t)e^{i\psi(t)} \equiv \frac{1}{N}\sum_{j=1}^{N} e^{i\phi_j(t)}. \tag{2.19}$$

Multiplying both sides of Eq. (2.19) by $e^{-i\phi_i}$ gives

$$re^{i(\psi-\phi_i)} = \frac{1}{N}\sum_{j=1}^{N} e^{i(\phi_j-\phi_i)}. \tag{2.20}$$

Taking imaginary part of Eq. (2.20)

$$r\sin(\psi-\phi_i) = \frac{1}{N}\sum_{j=1}^{N}\sin(\phi_j-\phi_i) \tag{2.21}$$

and inserting Eq. (2.21) into Eq. (2.18) induce

$$\dot{\phi}_i = \omega_i + Kr\sin(\psi - \phi_i). \tag{2.22}$$

By setting $\psi = 0$ in Eq. (2.19) and Eq. (2.22) without loss of generality we get

$$r = \frac{1}{N}\sum_{j=1}^{N} e^{i\phi_j(t)} \tag{2.23}$$

and

$$\dot{\phi}_i = \omega_i - Kr\sin\phi_i. \tag{2.24}$$

The solution of Eq. (2.24) exists when $|\omega_i| \leq Kr$. Let $\rho_\omega(\phi)\mathrm{d}\phi$ be the fraction of oscillators with phase between ϕ and $\phi + \mathrm{d}\phi$ among oscillators with natural frequency ω. Then,
For $|\omega| \leq Kr$,

$$\rho_\omega(\phi) = \delta\Big(\phi - \sin^{-1}\big(\frac{\omega}{Kr}\big)\Big), \tag{2.25}$$

For $|\omega| > Kr$,

$$\begin{aligned} \rho_\omega(\phi) &= \frac{C}{|\dot{\phi}|} \\ &= \frac{C}{|\omega - Kr\sin\phi|}, \end{aligned} \tag{2.26}$$

where C is a normalized constant determined from

$$\int_{-\pi}^{\pi} \rho_\omega(\phi)\mathrm{d}\phi = 1. \tag{2.27}$$

r can be thought as a sum of $r_{\rm lock}$ and $r_{\rm drift}$:

$$r = r_{\rm lock} + r_{\rm drift}. \tag{2.28}$$

$r_{\rm lock}$ is

$$\begin{aligned} r_{\rm lock} &= \langle e^{i\phi} \rangle_{\rm lock} \\ &= \int_{-Kr}^{Kr} e^{i\phi} g(\omega) \mathrm{d}\omega \\ &= \int_{-Kr}^{Kr} \cos\phi(\omega) g(\omega) \mathrm{d}\omega + i \cancel{\int_{-Kr}^{Kr} \sin\phi(\omega) g(\omega) \mathrm{d}\omega}, \end{aligned} \tag{2.29}$$

and $r_{\rm drift}$ is

$$\begin{aligned} r_{\rm drift} &= \langle e^{i\phi} \rangle_{\rm drift} \\ &= \langle \cos\phi \rangle_{\rm drift} + i \langle \sin\phi \rangle_{\rm drift}. \end{aligned} \tag{2.30}$$

Here, $\langle \cos\phi \rangle_{\rm drift}$ is zero because of

$$\begin{aligned} &\langle \cos\phi \rangle_{\rm drift} \\ &= \int_{-\pi}^{\pi} \int_{|\omega|>Kr} \cos\phi \rho_\omega(\phi) g(\omega) \mathrm{d}\omega \mathrm{d}\phi \qquad (2.31) \\ &= \int_{-\pi}^{0} \int_{-\infty}^{-Kr} \cos\phi \rho_\omega(\phi) g(\omega) \mathrm{d}\omega \mathrm{d}\phi \\ &\quad + \int_{-\pi}^{0} \int_{Kr}^{\infty} \cos\phi \rho_\omega(\phi) g(\omega) \mathrm{d}\omega \mathrm{d}\phi \\ &\quad + \int_{0}^{\pi} \int_{-\infty}^{-Kr} \cos\phi \rho_\omega(\phi) g(\omega) \mathrm{d}\omega \mathrm{d}\phi \\ &\quad + \int_{0}^{\pi} \int_{Kr}^{\infty} \cos\phi \rho_\omega(\phi) g(\omega) \mathrm{d}\omega \mathrm{d}\phi \qquad (2.32) \\ &= \int_{0}^{\pi} \int_{\infty}^{Kr} \cos(\phi'+\pi) \rho_{-\omega'}(\phi'+\pi) g(-\omega')(-1) \mathrm{d}\omega' \mathrm{d}\phi' \end{aligned}$$

$$
\begin{aligned}
&+\int_0^{\pi}\int_{-Kr}^{-\infty}\cos(\phi'+\pi)\rho_{-\omega'}(\phi'+\pi)g(-\omega')(-1)\mathrm{d}\omega'\mathrm{d}\phi' \\
&+\int_0^{\pi}\int_{-\infty}^{-Kr}\cos\phi\rho_{\omega}(\phi)g(\omega)\mathrm{d}\omega\mathrm{d}\phi \\
&+\int_0^{\pi}\int_{Kr}^{\infty}\cos\phi\rho_{\omega}(\phi)g(\omega)\mathrm{d}\omega\mathrm{d}\phi \qquad (2.33)\\
=&\cancel{\int_0^{\pi}\int_{\infty}^{Kr}\cos\phi'\rho_{\omega'}(\phi')g(\omega')(-1)\mathrm{d}\omega'\mathrm{d}\phi'} \\
&\cancel{+\int_0^{\pi}\int_{-Kr}^{-\infty}\cos(\phi')\rho_{\omega'}(\phi')g(\omega')(-1)\mathrm{d}\omega'\mathrm{d}\phi'} \\
&\cancel{+\int_0^{\pi}\int_{-\infty}^{-Kr}\cos\phi\rho_{\omega}(\phi)g(\omega)\mathrm{d}\omega\mathrm{d}\phi} \\
&\cancel{+\int_0^{\pi}\int_{Kr}^{\infty}\cos\phi\rho_{\omega}(\phi)g(\omega)\mathrm{d}\omega\mathrm{d}\phi} \\
=&\,0. \qquad (2.34)
\end{aligned}
$$

We used change of variables $\phi = \phi' + \pi$ ($\mathrm{d}\phi = \mathrm{d}\phi'$), $\omega = -\omega'$ ($\mathrm{d}\omega = -\mathrm{d}\omega'$) for 1st and 2nd term of Eq. (2.32) and the property $\rho_{\omega}(\phi) = \rho_{-\omega}(\phi+\pi)$ derived from Eq. (2.26) and $g(\omega) = g(-\omega)$ at Eq. (2.33). Similarly we get also $\langle \sin\phi \rangle_{\mathrm{drift}} = 0$, therefore, Eq. (2.30) leads to

$$
r_{\mathrm{drift}} \;=\; 0. \qquad (2.35)
$$

2.4.1 Case of random sampling

In this subsection, we follow the processes introduced in [30]. Inserting Eq. (2.29) and Eq. (2.35) into Eq. (2.28) and using $\omega = Kr\sin\phi$ in the steady state lead to,

$$
\begin{aligned}
r &= \int_{-Kr}^{Kr}\cos\phi g(\omega)\mathrm{d}\omega \\
&= \int_{-\frac{\pi}{2}}^{\frac{\pi}{2}}\cos\phi g(Kr\sin\phi)Kr\cos\phi\mathrm{d}\phi
\end{aligned}
$$

$$
\begin{aligned}
&= Kr\int_{-\frac{\pi}{2}}^{\frac{\pi}{2}}\cos^2\phi g(Kr\sin\phi)\mathrm{d}\phi \qquad (2.36)\\
&= Kr\int_{-\frac{\pi}{2}}^{\frac{\pi}{2}}\cos^2\phi\Big(g(0)+\cancel{g'(0)Kr\sin\phi}+\frac{g''(0)}{2}(Kr\sin\phi)^2\\
&\qquad +\cancel{\frac{g'''(0)}{6}(Kr\sin\phi)^3}+\cdots\Big)\mathrm{d}\phi\\
&= Kr\Big[\int_{-\frac{\pi}{2}}^{\frac{\pi}{2}}\cos^2\phi g(0)\mathrm{d}\phi+\int_{-\frac{\pi}{2}}^{\frac{\pi}{2}}\cos^2\phi\frac{g''(0)}{2}(Kr\sin\phi)^2\mathrm{d}\phi+\cdots\Big]\\
&= \frac{\pi}{2}g(0)Kr+\frac{\pi}{16}g''(0)K^3r^3+O(r^5). \qquad (2.37)
\end{aligned}
$$

At $K=K_{\mathrm{c}}$, $r=0^+$, so Eq. (2.36) is reduced to

$$
\begin{aligned}
1 &= K\int_{-\frac{\pi}{2}}^{\frac{\pi}{2}}\cos^2\phi g(Kr\sin\phi)\mathrm{d}\phi\\
&= K_{\mathrm{c}}\int_{-\frac{\pi}{2}}^{\frac{\pi}{2}}\cos^2\phi g(0)\mathrm{d}\phi\\
&= K_{\mathrm{c}}\frac{\pi}{2}g(0). \qquad (2.38)
\end{aligned}
$$

Hence, we get the critical coupling strength as

$$
K_{\mathrm{c}} = \frac{2}{\pi g(0)}. \qquad (2.39)
$$

By inserting Eq. (2.39) into Eq. (2.37), we obtain self-consistency equation for order parameter:

$$
\begin{aligned}
r &= \frac{K}{K_{\mathrm{c}}}r+\frac{\pi}{16}g''(0)K^3r^3+O(r^5)\\
&\equiv aKr-cK^3r^3+\delta\tilde{\Psi}_N, \qquad (2.40)
\end{aligned}
$$

where $\delta\tilde{\Psi}_N\equiv\tilde{\Psi}_N(r)-\Psi(r)$. $\Psi(r)$ and $\tilde{\Psi}_N(r)$ are defined as

$$
r = \int_{-Kr}^{Kr}\cos\phi g(\omega)\mathrm{d}\omega
$$

$$
\begin{aligned}
&= \int_{-Kr}^{Kr} g(\omega)\sqrt{1-\Big(\frac{\omega}{Kr}\Big)^2}\,\mathrm{d}\omega \\
&\equiv \Psi(r) \qquad (2.41)
\end{aligned}
$$

and

$$
\begin{aligned}
r(N) &= \frac{1}{N}\sum_{j,|\omega_j|<Kr}\cos\phi_j \\
&= \frac{1}{N}\sum_j \sqrt{1-\Big(\frac{\omega_j}{Kr}\Big)^2}\,\Theta\Big(1-\frac{|\omega_j|}{Kr}\Big) \\
&\equiv \tilde{\Psi}_N(r), \qquad (2.42)
\end{aligned}
$$

where Θ is the Heaviside step function.

$\tilde{\Psi}_N(r)$ can be considered as a mean value of N random numbers which are extracted from $\eta(\omega)$,

$$
\eta(\omega) = \sqrt{1-\Big(\frac{\omega}{Kr}\Big)^2}\,\Theta\Big(1-\frac{|\omega|}{Kr}\Big). \qquad (2.43)
$$

The variance of η is

$$
\begin{aligned}
\mathrm{Var}[\eta] &= \langle\eta^2\rangle - \langle\eta\rangle^2 \\
&= \int_{-Kr}^{Kr} g(\omega)\Big[1-\Big(\frac{\omega}{Kr}\Big)^2\Big]\mathrm{d}\omega - \cancel{(\Psi(r))^2} \to 0^+ \text{ for } K_\mathrm{c} \\
&\approx \int_{-Kr}^{Kr}\Big(g(0)+\frac{1}{2}g''(0)\omega^2+\cdots\Big)\Big[1-\Big(\frac{\omega}{Kr}\Big)^2\Big]\mathrm{d}\omega \\
&= \frac{4}{3}g(0)Kr + O(r^2). \qquad (2.44)
\end{aligned}
$$

Therefore, the variance of $\tilde{\Psi}_N(r)$ is $\mathrm{Var}[\tilde{\Psi}_N(r)] = \frac{4}{3}g(0)Kr/N + O(r^2/N)$

and $\mathrm{Std}[\tilde{\Psi}_N(r)] \approx \sqrt{\frac{4}{3}g(0)Kr/N}$. At $K = K_c$, Eq. (2.40) becomes

$$\begin{aligned} cK^3r^3 &= \delta\tilde{\Psi}_N \\ r^3 &\sim \delta\tilde{\Psi}_N \sim \mathrm{Std}[\tilde{\Psi}_N(r)] \sim \sqrt{r/N}. \end{aligned} \tag{2.45}$$

Let $r \sim N^{-a}$, then $r^3 \sim N^{-3a} \sim \sqrt{N^{-a-1}}$. We get $a = 1/5$ and

$$r(K = K_c) \sim N^{-1/5}. \tag{2.46}$$

Near $K \sim K_c$, Eq. (2.40) becomes

$$\begin{aligned} cK^3r^3 &= \epsilon r + \cancel{\delta\tilde{\Psi}_N} \\ r^2 &\sim \epsilon \\ r &\sim \epsilon^{1/2}, \end{aligned} \tag{2.47}$$

where $\epsilon \equiv (K - K_c)/K_c$.

Combining Eq. (2.46) and Eq. (2.47), we can write the scaling form

$$r(K, N) = N^{-1/5} f(\epsilon N^{2/5}), \tag{2.48}$$

where $f(x)$ is a scaling function and $f(x) \sim$ const when $x \to 0$, $f(x) \sim x^{1/2}$ when $x > 0$.

By inserting Eq. (2.48) into Eq. (2.40) and using $x \equiv \epsilon N^{2/5} (\epsilon \sim xN^{-2/5})$ and Eq. (2.39), we get

$$\begin{aligned} &\epsilon N^{-1/5} f(x) - cK^3 N^{-3/5} f^3(x) + (\frac{4}{3} g(0) K N^{-6/5} f(x))^{1/2} \mu = 0 \\ &x\cancel{N^{-3/5}} f(x) - cK^3 \cancel{N^{-3/5}} f^3(x) + (\frac{4}{3}\frac{2}{\pi K_c} K \cancel{N^{-6/5}} f(x))^{1/2} \mu = 0, \end{aligned} \tag{2.49}$$

where $\mu \equiv \delta\tilde{\Psi}/\langle(\delta\tilde{\Psi})^2\rangle^{1/2}$ is a random variable from Gaussian distribution with unit variance and zero-mean.

Then, near $K \sim K_{\rm c}$ we get

$$xf(x) - cK_{\rm c}{}^3 f^3(x) + (\frac{8}{3\pi})^{1/2}\mu f^{1/2}(x) = 0. \tag{2.50}$$

2.4.2 Case of regular sampling

Regular sampling of natural frequencies from Gaussian distribution is expressed as

$$\omega_j = \sqrt{2\sigma^2}\mathrm{erf}^{-1}\left(-1+\frac{2j-1}{N}\right), \quad j = 1, \cdots, N. \tag{2.51}$$

Now, we renumber the index of oscillators for more mathematical tractability as

$$\omega_{\pm j} = \pm\sqrt{2\sigma^2}\mathrm{erf}^{-1}\left(\frac{2j-1}{N}\right), \quad j = 1, \cdots, N/2, \tag{2.52}$$

where we assumed that N is an even number.

From Eq. (2.35), we know that drifting oscillators' contribution to order parameter is zero. Therefore,

$$\begin{aligned} r &= r_{\rm lock} + \cancel{r_{\rm drift}} \\ &= \frac{2}{N}\sum_{i=1}^{n}\cos\phi_i \\ &= \frac{2}{N}\sum_{i=1}^{n}\sqrt{1-\left(\frac{\omega_i}{Kr}\right)^2} \qquad (2.53) \\ &\equiv \frac{2}{N}\sum_{i=1}^{n} f(i), \qquad (2.54) \end{aligned}$$

where n is the index satisfying $\omega_n \leq Kr < \omega_{n+1}$. And we used the fact $\omega_i - Kr\sin\phi_i = 0$ in the steady state.

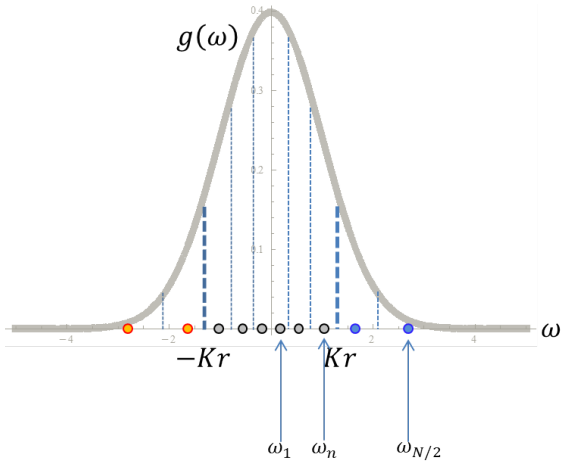

Figure 2.13: Locked oscillators and drifting oscillators in a case of regular sampling.

By applying Euler-Maclaurin formula,

$$\sum_{i=m}^{n} f(i) \simeq \int_{m}^{n} f(x)\mathrm{d}x + \frac{1}{2}f(n) + \frac{1}{2}f(m) \tag{2.55}$$

to Eq. (2.54) we get

$$\begin{aligned} r &= \frac{2}{N}\Big(\int_{1}^{n} f(x)\mathrm{d}x + \frac{1}{2}f(n) + \frac{1}{2}f(1)\Big) && (2.56)\\ &\equiv \frac{2}{N}\Big(A + B + C\Big). && (2.57) \end{aligned}$$

Before going to further process, some useful approximations and formula about error function are introduced:

$$\mathrm{erf}(x) \simeq \frac{2}{\sqrt{\pi}}x - \frac{2}{3\sqrt{\pi}}x^3 + O(x^5) \tag{2.58}$$

$$\mathrm{erf}^{-1}(x) \simeq \frac{\sqrt{\pi}}{2}x + \frac{\pi^{\frac{3}{2}}}{24}x^3 + O(x^5) \tag{2.59}$$

$$\frac{\mathrm{d}}{\mathrm{d}x}\mathrm{erf}(x) = \frac{2}{\sqrt{\pi}}e^{-x^2} \tag{2.60}$$

From now on, we set $\sigma = 1$ in Eq. (2.52). Then it leads to

$$\omega_n \leq Kr < \omega_{n+1} \tag{2.61}$$

$$\sqrt{2}\mathrm{erf}^{-1}\Big(\frac{2n-1}{N}\Big) \leq Kr < \sqrt{2}\mathrm{erf}^{-1}\Big(\frac{2n+1}{N}\Big)$$

$$\frac{N\mathrm{erf}(\frac{Kr}{\sqrt{2}})-1}{2} < n \leq \frac{N\mathrm{erf}(\frac{Kr}{\sqrt{2}})+1}{2}. \tag{2.62}$$

So we get the index n as a function of K, r and N:

$$n = \left[\frac{N\mathrm{erf}(\frac{Kr}{\sqrt{2}})+1}{2}\right] \simeq \frac{N\mathrm{erf}(\frac{Kr}{\sqrt{2}})}{2}. \tag{2.63}$$

And we know

$$\omega_1 = \sqrt{2}\mathrm{erf}^{-1}\Big(\frac{1}{N}\Big) \tag{2.64}$$

$$\simeq \sqrt{\frac{\pi}{2}}\frac{1}{N} \tag{2.65}$$

and

$$\omega_n = \sqrt{2}\mathrm{erf}^{-1}\Big(\frac{2n-1}{N}\Big) \tag{2.66}$$

$$\simeq \sqrt{2}\mathrm{erf}^{-1}\Big(\frac{N\mathrm{erf}(\frac{Kr}{\sqrt{2}})-1}{N}\Big)$$

$$\simeq \sqrt{2}\mathrm{erf}^{-1}\Big(\frac{2}{\sqrt{\pi}}\frac{Kr}{\sqrt{2}} - \frac{1}{N}\Big)$$

$$\simeq \sqrt{2}\frac{\sqrt{\pi}}{2}\Big(\sqrt{\frac{2}{\pi}}Kr - \frac{1}{N}\Big)$$

$$= Kr - \sqrt{\frac{\pi}{2}}\frac{1}{N} \tag{2.67}$$

$$= \quad Kr - \omega_1. \tag{2.68}$$

Let's calculate Eq. (2.57) term by term. The first term is

$$\begin{aligned} A &\equiv \int_1^n f(x)\mathrm{d}x && (2.69)\\ &= \int_1^n \sqrt{1-\Big(\frac{\omega_x}{Kr}\Big)^2}\mathrm{d}x && (2.70)\\ &= \int_{\omega_1}^{\omega_n} \sqrt{1-\Big(\frac{\omega_x}{Kr}\Big)^2}\frac{N}{\sqrt{2\pi}}e^{-\frac{{\omega_x}^2}{2}}\mathrm{d}\omega_x && (2.71)\\ &= \frac{N}{\sqrt{2\pi}}\int_{\omega_1}^{\omega_n} \sqrt{1-\Big(\frac{\omega}{Kr}\Big)^2}e^{-\frac{\omega^2}{2}}\mathrm{d}\omega, && (2.72) \end{aligned}$$

where we used

$$\begin{aligned} &\omega_x = \sqrt{2}\mathrm{erf}^{-1}\Big(\frac{2x-1}{N}\Big) && (2.73)\\ &\mathrm{erf}\Big(\frac{\omega_x}{\sqrt{2}}\Big) = \frac{2x-1}{N} && (2.74)\\ &\frac{2}{\sqrt{\pi}}e^{-\frac{{\omega_x}^2}{2}}\frac{1}{\sqrt{2}}\mathrm{d}\omega_x = \frac{2}{N}\mathrm{d}x && (2.75)\\ \therefore \quad &\mathrm{d}x = N\frac{1}{\sqrt{2\pi}}e^{-\frac{{\omega_x}^2}{2}}\mathrm{d}\omega_x. && (2.76) \end{aligned}$$

We devide Eq. (2.76) into three terms as

$$\begin{aligned} A &= \frac{N}{\sqrt{2\pi}}\int_0^{Kr} \sqrt{1-\Big(\frac{\omega}{Kr}\Big)^2}e^{-\frac{\omega^2}{2}}\mathrm{d}\omega && (2.77)\\ &\quad -\frac{N}{\sqrt{2\pi}}\int_0^{\omega_1} \sqrt{1-\Big(\frac{\omega}{Kr}\Big)^2}e^{-\frac{\omega^2}{2}}\mathrm{d}\omega && (2.78)\\ &\quad -\frac{N}{\sqrt{2\pi}}\int_{\omega_n}^{Kr} \sqrt{1-\Big(\frac{\omega}{Kr}\Big)^2}e^{-\frac{\omega^2}{2}}\mathrm{d}\omega && (2.79)\\ &\equiv A1 - A2 - A3. && (2.80) \end{aligned}$$

The first term of Eq. (2.80) is

$$
\begin{aligned}
A1 &\equiv \frac{N}{\sqrt{2\pi}}\int_0^{Kr}\sqrt{1-\Big(\frac{\omega}{Kr}\Big)^2}e^{-\frac{\omega^2}{2}}\mathrm{d}\omega && (2.81)\\
&= \frac{N}{\sqrt{2\pi}}\frac{1}{4}e^{-\frac{K^2r^2}{4}}Kr\pi\bigg(J_0\Big(\frac{K^2r^2}{4}\Big)+J_1\Big(\frac{K^2r^2}{4}\Big)\bigg)\\
&\simeq \frac{N}{\sqrt{2\pi}}\frac{\pi}{4}Kr\Big(1-\frac{K^2r^2}{4}\Big)\Big(1+\frac{K^2r^2}{8}\Big)\\
&\simeq \frac{N}{\sqrt{2\pi}}\frac{\pi}{4}Kr\Big(1-\frac{K^2r^2}{8}\Big), && (2.82)
\end{aligned}
$$

where the following approximations of Bessel functions (J_0 and J_1) are used:

$$
\begin{aligned}
J_0(x) &\simeq 1+\frac{x^2}{4}+O(x^4) && (2.83)\\
J_1(x) &\simeq \frac{x}{2}+\frac{x^3}{16}+O(x^5). && (2.84)
\end{aligned}
$$

The second term of Eq. (2.80) is

$$
\begin{aligned}
A2 &\equiv \frac{N}{\sqrt{2\pi}}\int_0^{\omega_1}\sqrt{1-\Big(\frac{\omega}{Kr}\Big)^2}e^{-\frac{\omega^2}{2}}\mathrm{d}\omega && (2.85)\\
&\simeq \frac{N}{\sqrt{2\pi}}\int_0^{\omega_1}\Big(1-\frac{1}{2}\Big(\frac{\omega}{Kr}\Big)^2\Big)e^{-\frac{\omega^2}{2}}\mathrm{d}\omega\\
&= \frac{N}{\sqrt{2\pi}}\Big(\frac{e^{-\frac{\omega_1^2}{2}}\omega_1}{2K^2r^2}+\frac{(-1+2K^2r^2)\sqrt{2\pi}\mathrm{erf}(\frac{\omega_1}{\sqrt{2}})}{4K^2r^2}\Big)\\
&\simeq \frac{N}{\sqrt{2\pi}}\Big(\cancel{\frac{\omega_1}{2K^2r^2}}-\cancel{\frac{2\omega_1}{4K^2r^2}}+\omega_1\Big)\\
&\simeq \frac{1}{2}. && (2.86)
\end{aligned}
$$

And by applying change of variables, $t\equiv\frac{\omega}{Kr}, \mathrm{d}t=\frac{\mathrm{d}\omega}{Kr}$ and $t_i=\frac{Kr-\omega_1}{Kr}\equiv 1-\eta$,

$t_f = \frac{Kr}{Kr} = 1$, we can calculate the last term of Eq. (2.80):

$$\begin{aligned} A3 &\equiv \frac{N}{\sqrt{2\pi}} \int_{\omega_1}^{Kr} \sqrt{1 - \Big(\frac{\omega}{Kr}\Big)^2} e^{-\frac{\omega^2}{2}} \mathrm{d}\omega && (2.87) \\ &= \frac{N}{\sqrt{2\pi}} \int_{1-\eta}^{1} e^{-\frac{K^2 r^2 t^2}{2}} \sqrt{1-t^2} Kr \mathrm{d}t \\ &= \frac{NKr}{\sqrt{2\pi}} \int_{1-\eta}^{1} \sqrt{1-t} \Big(e^{-\frac{K^2 r^2 t^2}{2}} \sqrt{1+t} \Big) \mathrm{d}t \\ &\simeq \frac{NKr}{\sqrt{2\pi}} \sqrt{2} e^{-\frac{K^2 r^2}{2}} \int_{1-\eta}^{1} \sqrt{1-t} \mathrm{d}t \\ &= \frac{2}{3} \frac{1}{\sqrt{\pi}} \Big(\frac{\pi}{2}\Big)^{\frac{3}{4}} e^{-\frac{K^2 r^2}{2}} (NKr)^{-\frac{1}{2}}. && (2.88) \end{aligned}$$

The second term and third term of Eq. (2.57) are

$$\begin{aligned} B &\equiv \frac{1}{2} f(n) && (2.89) \\ &= \frac{1}{2} \sqrt{1 - \Big(\frac{\omega_n}{Kr}\Big)^2} \\ &\simeq \frac{1}{2} \frac{(2\pi)^{\frac{1}{4}}}{\sqrt{Nkr}} && (2.90) \end{aligned}$$

and

$$\begin{aligned} C &\equiv \frac{1}{2} f(1) && (2.91) \\ &= \frac{1}{2} \sqrt{1 - \Big(\frac{\omega_1}{Kr}\Big)^2} \\ &\simeq \frac{1}{2} \Big(1 - \frac{\pi}{4N^2 K^2 r^2}\Big), && (2.92) \end{aligned}$$

respectively.

Gathering these terms (Eq. (2.82), Eq. (2.86), Eq. (2.88), Eq. (2.90) and

Eq. (2.92)) all together leads to

$$\begin{aligned} r &= \frac{2}{N}(A+B+C) \\ &= \frac{2}{N}(A1-A2-A3+B+C) \\ &\simeq \sqrt{\frac{\pi}{8}}Kr - \sqrt{\frac{\pi}{8}}\frac{K^3r^3}{8} \\ &\quad + \Big((2\pi)^{\frac{1}{4}} - \frac{4}{3}\frac{1}{\sqrt{\pi}}(\frac{\pi}{2})^{\frac{3}{4}}\Big)\frac{1}{\sqrt{Kr}N^{\frac{3}{2}}}. \end{aligned} \tag{2.93}$$

Finally, inserting $K = K_c = \sqrt{\frac{8}{\pi}}$ gives the answer:

$$\begin{aligned} r^{\frac{7}{2}} &\sim N^{-\frac{3}{2}} \\ \therefore r &\sim N^{-\frac{3}{7}}. \end{aligned} \tag{2.94}$$

Unfortunately $\beta/\bar{\nu} \approx 3/8$ obtained by simulating the Kuramoto model and $\beta/\bar{\nu} \approx 3/7$ from analytic solution do not coincide. The main factor that influences the discrepancy between two solutions is *fuzzy oscillators* [10]. When we calculated the finite-size effect of coupled oscillators for the case of regular sampling, we assumed that there are only two kinds of oscillators in the steady state: *locked oscillators* and *drifting oscillators*. In real dynamics, however, the order parameter has fluctuations even though the system is in the steady states, which in turn make the role of fuzzy oscillators important. Taking the role of fuzzy oscillators into account remains an important problem.

2.5 n-dimensional square lattice

The authors of [21, 29] discovered that the lower critical dimension $d_l^P = 4$ for phase synchronization. That means oscillators on square lattice whose dimension ≤ 4 are not synchronized with finite coupling strength. Here we consider the thermodynamic limit $N \to \infty$. Even though some finite oscillators are synchronized for given K, larger systems might not be synchronized for that K. This is because the drifting (or runaway) oscillators break up the synchronization under the lower critical dimension ($d \leq d_l^p$). In other words, the phase synchronization occurs from 5 dimension. For frequency synchronization, on the other hand, the lower critical dimension $d_l^F = 2$ [21] indicating that the frequency synchronization (frequency entrainment) occurs from three dimension.

Some previous studies on finite-size scaling of phase synchronization are summarized in Table 2.2 (square lattice) and Table 2.4 (fully-connected network, scale-free network).

Table 2.2: Critical exponents of finite-size scaling for square lattice.

Model	d	β	ν	β/ν	K_c	Ref.	Etc.
KM on square lattice 1	5	-	0.45(10)	1.5(3)	0.200(5)	[29], [21]	numeric
	6	-	0.45(10)	1.0(3)	0.156(2)		
KM on square lattice 2	$d>4$	$\frac{1}{2}$	$\frac{5}{2d}$	$\frac{d}{5}$	-	[30]	numeric ($d=5,6$)
	$2<d\leq 4$	0	$\frac{2}{d-2}$	0	-		numeric, analytic
KM on square lattice 3	$d>4$	$\frac{1}{2}$	$\frac{5}{2d}$	$\frac{d}{5}$	-	[49]	numeric
	$d\leq 4$	0	$\frac{2}{d-2}$	0	-		

Table 2.3: Symbols for networks.

Symbol	Network
FCN	fully-connected network
SF	scale-free
ER	Erdös-Rényi
RR	random-regular
LTC	square lattice

Table 2.4: Critical exponents of finite-size scaling for networks.

Model	β	$\bar{\nu}$	$\beta/\bar{\nu}$	γ for SF	Ref.	Etc.
KM on FCN	1/2	2	-	-	[50], [45]	analytic
	1/2	2.4(2)	-	-	[21]	numeric
	$\frac{1}{2}$	$\frac{5}{2}$	$\frac{1}{5}$	-	[30]	analytic
KM on FCN + wGSR	$\frac{1}{2}$	$\frac{5}{4}$	$\frac{2}{5}$	-	[18]	numeric
KM + thermal noise on FCN	$\frac{1}{2}$	2	$\frac{1}{4}$	-	[18]	numeric
KM on SF 1	$\frac{1}{2}$	2	$\frac{1}{4}$	$\gamma > 5$	[51]	analytic
	$\frac{1}{\gamma-3}$	$\frac{\gamma-1}{\gamma-3}$	$\frac{1}{\gamma-1}$	$3 < \gamma < 5$		
KM on SF 2	$\frac{1}{2}$	$\frac{5}{2}$	$\frac{1}{5}$	$\gamma > 5$	[42]	analytic
	$\frac{1}{\gamma-3}$	$\frac{2\gamma-5}{\gamma-3}$	$\frac{1}{2\gamma-5}$	$4 < \gamma < 5$		
	$\frac{1}{\gamma-3}$	$\frac{\gamma-1}{\gamma-3}$	$\frac{1}{\gamma-1}$	$3 < \gamma < 4$		
KM on SF 3	$\frac{1}{2}$	2	$\frac{1}{4}$	$\gamma > 5$	[13]	analytic, $\eta = 1$
	$\frac{1}{\gamma-3}$	$\frac{\gamma-1}{\gamma-3}$	$\frac{1}{\gamma-1}$	$3 < \gamma < 5$		
	$\frac{1}{3-\gamma}$	$\frac{2}{3-\gamma}$	$\frac{1}{2}$	$2 < \gamma < 3$		
	$\frac{\gamma-1}{3-\gamma}$	$\frac{2(\gamma-1)}{3-\gamma}$	$\frac{1}{2}$	$\gamma < 2$		

2.6 Summary

In numerical simulations with finite system size for the Kuramoto dynamics, one usually measure order parameter, susceptibility (which is related to standard deviation) and Binder's cumulant after the system goes to the steady state. We verified the finite-size effects on these measurable quantities and the scaling functions on near and at the criticality. A static thermodynamic exponent $\beta/\bar{\nu}$ was estimated from order parameter's dependence on system size. We confirmed the frequency-disorder fluctuation affects to the thermodynamic exponent both numerically and analytically. And susceptibility, standard deviation and Binder's cumulant are also tested with two kinds of sampling methods for natural frequencies. Moreover, it was confirmed that the self-averageness is affected by the sampling method for natural frequencies. In next chapter we will approach these features in another way, dynamic scaling.

Chapter 3

Dynamic Scaling

3.1 Motivation for dynamic scaling

To obtain time-averaged value of order parameter $\langle r \rangle$ (or r_{sat}), one usually discard the early-time data and take only the late-time data. In early time, $r(t)$ starts from its initial value r_0 and is going toward its saturated value r_{sat} but is not converged yet. When one collects data for r_{sat}, to estimate how many steps one should iterate for the numerical integration is required. Without the information about t_{sat}, one cannot decide the number of steps for numerical integration and be sure about the accuracy of data.

Here we focus on the values of $r(t)$ before the system enters the steady state. It is already known that $r(t)$ grows exponentially, $r(t) \sim \exp(at)$ before r saturates to r_∞ in supercritical regime ($K \gg K_{\mathrm{c}}$) [52, 53]. In a subcritical regime ($K \ll K_{\mathrm{c}}$), $r(t)$ does not grow enough but fluctuates near 0 by as much as $O(N^{-1/2})$.

Then one question follows naturally: How does $r(t)$ evolve at $K = K_{\mathrm{c}}$ or near $K = K_{\mathrm{c}}$? This is a main topic of this chapter.

3.2 Temporal behavior of order parameter near critical coupling strength

The direct observation of order parameter's temporal behavior is the first step of this study. We measured $r(t)$ with several coupling strength K near

K_c and plotted it in log-log scale. The system size is $N = 819,200$. We found that $r(t)$ shows the power-law behavior as $r(t) \sim t^{-y}$ when $K = K_c = \sqrt{8/\pi} \approx 1.595769$ in Fig. 3.1 (See triangles). For the initial condition of ϕ_i, we set $\phi_i(0) = \text{const}$ for all i that means $r(0) = 1$. The lower panel of Fig. 3.1 is a local slope of the upper one. The curve of $K = K_c$ has the longest flat regime before the curve saturated to r_{sat} compared to other K values. In other words, $r(t)$ decays following a power-law at $K = K_c$. When $K < K_c$ or $K > K_c$, on the other hand, $r(t)$ saturates fast. This is a signature of the *critical slowing down*. In Fig. 3.2 we plot r *vs.* t for several N at the criticality.

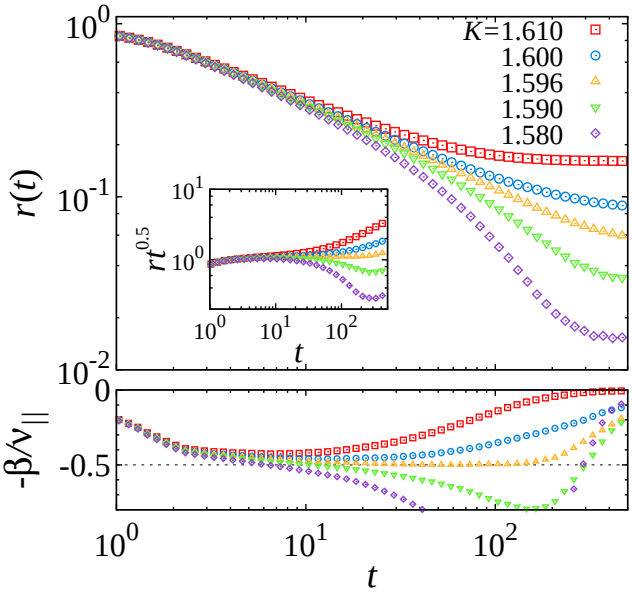

Figure 3.1: Time evolution of r near $K = K_c = \sqrt{8/\pi}$ with natural frequencies chosen randomly from Gaussian distribution whose $\sigma^2 = 1$. The upper panel shows $[r]$ *vs.* t and the inset is $t^{0.5}[r]$ *vs.* t. The initial phases are all same, $\phi_i(0)$=const for all i, therefore $r(0)$=1. The system size N is 819,200. The number of configurations for $\{\omega_i\}$ is 200. The lower panel is a local slope of the upper one.

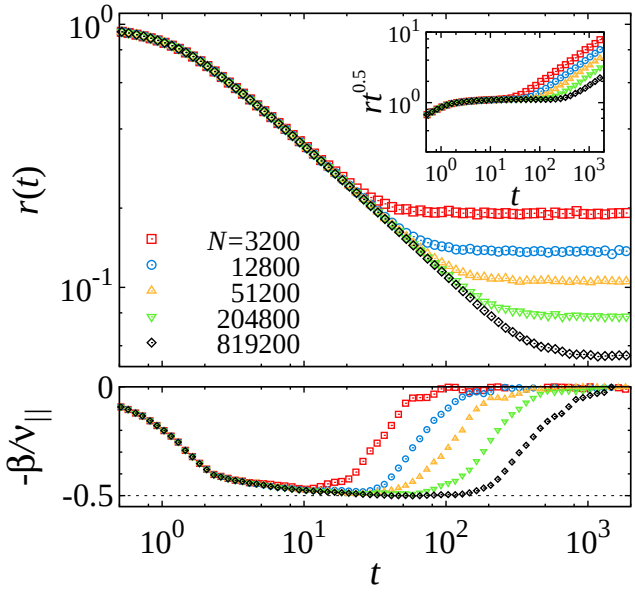

Figure 3.2: (top) Time evolution of r at $K = K_c = \sqrt{8/\pi}$ with natural frequencies chosen randomly from Gaussian distribution. The initial phases are all same, $r(0)$=1. The number of ensemble is 500 for $N \leq$51200, 200 for $N \geq$204800. (bottom) The local slope of the main graph.

3.3 What is dynamic scaling?

Let's start from some physical quantity $w(t)$ (for example, interface width in surface growth problem) which increases or decreases following a power-law of time as $w(t) \sim t^{\theta}$. For finite system $w(t)$ might saturate to some value (Let's call it w_{sat}, saturation value of w) at $t = t_{\text{sat}}$. The saturation value w_{sat} is a power function of system size: $w_{\text{sat}} \sim L^{\alpha}$. Similarly the saturation time t_{sat} is also a power function of system size: $t_{\text{sat}} \sim L^{z}$. We call θ, α and z as growth exponent, roughness exponent and dynamic exponent, respectively. Three exponents are related with scaling law, $z = \alpha/\theta$ [20]. Then, w *vs.* t graphs for several system sizes can be collapsed in a single curve as w/L^{α} *vs.* t/L^{z} from which we know that a scaling relation $w(L,t) = L^{\alpha} f(t/L^{z})$ exists. Here, $f(x)$ is a scaling function. It behaves as $f(x) \sim x^{\theta}$ for $x \ll 1$ and $f(x) \sim \text{const}$ for $x \gg 1$.

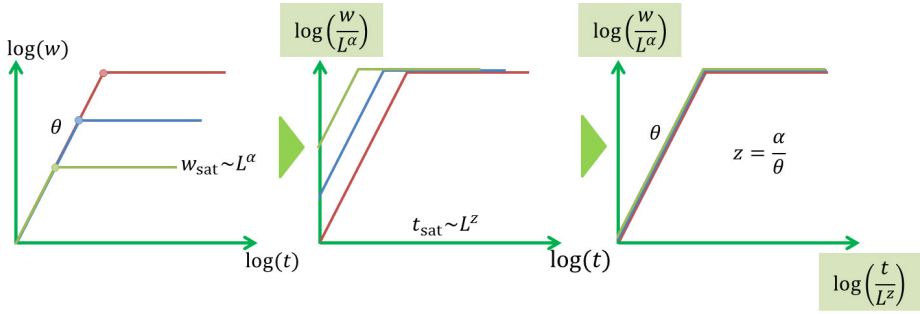

Figure 3.3: Schematic diagram for dynamic scaling.

Another possible scaling form is $w(L,t) = t^{\theta} g(t/L^{z})$. In this case, the scaling function $g(x)$ behaves as $g(x) \sim \text{const}$ for $x \ll 1$ and $g(x) \sim x^{-\theta}$ for $x \gg 1$. Using these dynamic scaling relations, one can find thermodynamic exponents numerically.

3.4 Dynamic scaling with random sampling

We found that the dynamic scaling exists at critical point, $K = K_c$. Two kinds of initial conditions (ordered state and disordered state) for phases $\{\phi\}$ are considered. The first one is $\phi_i(0) = \text{const}$ for all i that means ordered state, $r_0 = 1$. And the second one is randomly assigned $\phi_i(0) \in [0, 2\pi)$ for all i that means disordered state, $r_0 \sim 1/\sqrt{N}$.

Note that r_{sat} (the saturated value of r) does not depend on the two kinds of initial conditions for phase. It is guaranteed by the fact that the Kuramoto model exhibits a second order phase transition. r_{sat}, of course, depend on the sample-to-sample fluctuation of natural frequencies. Therefore, we need to average r_{sat} over different configurations for natural frequencies.

3.4.1 Starting from ordered state, $r(0) = 1$

Let's start from the first condition $r(0) = 1$. Considering $r_{\text{sat}} \sim N^{-\beta/\bar{\nu}}$ which is from the finite-size scaling and $t_{\text{sat}} \sim N^{\bar{z}}$, we can conjecture the dynamic scaling form at $K = K_c$ as following,

$$r(t, N, K_c) = N^{-\beta/\bar{\nu}} h_1(t/N^{\bar{z}}), \tag{3.1}$$

where $h_1(x) \sim \text{constant}$ for $x \gg 1$ and $h_1(x) \sim x^{-y}$ for $x \to 0$. For any finite values of N, $r(N)$ saturates to some value proportional to $N^{-\beta/\bar{\nu}}$ in the limit of $t \to \infty$. And in the limit of $N \to \infty$, $r(t)$ should not depend on N at finite time t. So $-\beta/\bar{\nu} + \bar{z}y = 0$, hence we get $y = \beta/(\bar{\nu}\bar{z}) = \frac{\beta}{\nu_\parallel}$. In the last equality we used $\bar{z} \equiv \nu_\parallel/\bar{\nu}$, $\nu_\parallel$ is from $t_{\text{sat}} \sim (K - K_c)^{-\nu_\parallel}$.

In Fig.3.4 we plot Eq. (3.1). The upper figure is the best collapsed case with $\beta/\bar{\nu} = 0.220$ and $\bar{z} = 0.432$. The theoretical values of the exponents are

$\beta/\bar{\nu} = 0.2$ and $\bar{z} = 0.4$. The lower figure was drawn using these theoretical values.

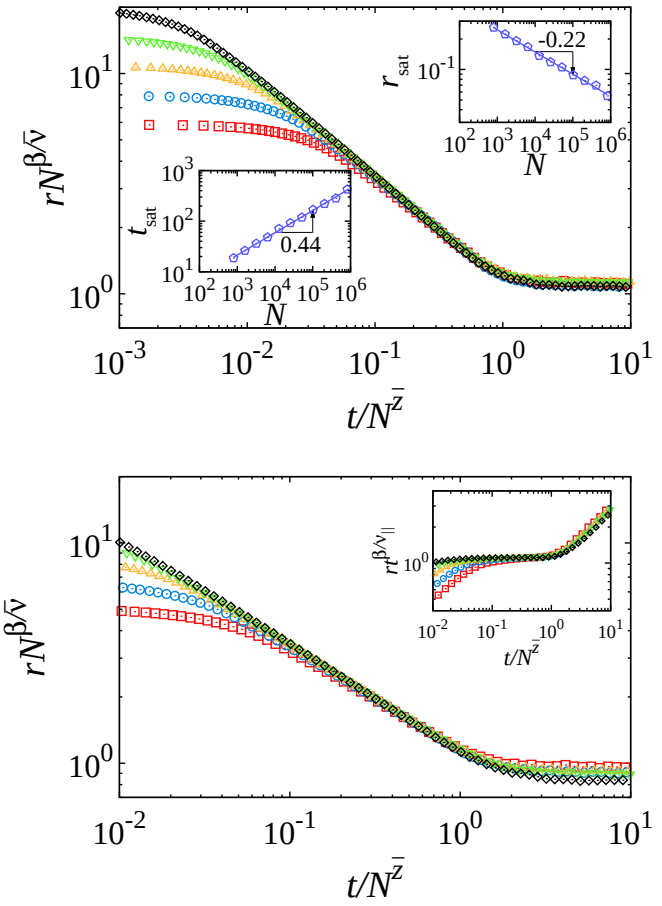

Figure 3.4: Dynamic scaling. $rN^{\beta/\bar{\nu}} vs. t/N^{\bar{z}}$ (top) dynamic scaling function h_1 with exponents found in its insets. The curves for different sizes collapse into one single curve. (inset) $t_{\rm sat} vs. N$ and $r_{\rm sat} vs. N$ in log-log scale. The slopes mean $\bar{z}$ and $-\beta/\bar{\nu}$, respectively. We found $\beta/\bar{\nu}$=0.220, $\bar{z}$=0.432. (bottom) dynamic scaling function h_1 with theoretical value $\beta/\bar{\nu}$=0.2, $\bar{z}$=0.4 (inset) dynamic scaling function h_2.

Another dynamic scaling form is

$$r(t, N, K_{\rm c}) = t^{-\beta/\nu_\parallel} h_2(t/N^{\bar{z}}), \tag{3.2}$$

where $h_2(x) \sim x^y$ for $x \gg 1$ and $h_2(x) \sim$ constant for $x \to 0$. For any finite values of N, $r(N)$ saturates to some value proportional to $N^{-\beta/\bar{\nu}}$ in the limit of $t \to \infty$. Therefore we obtain $y = \beta/\nu_{\|}$ which is same with the result from the first dynamic scaling relation. See the inset of lower panel in Fig. 3.4.

Fig. 3.5 shows that $\nu_{\|} = 1$ and $\beta = 1/2$ for fully-connected networks.

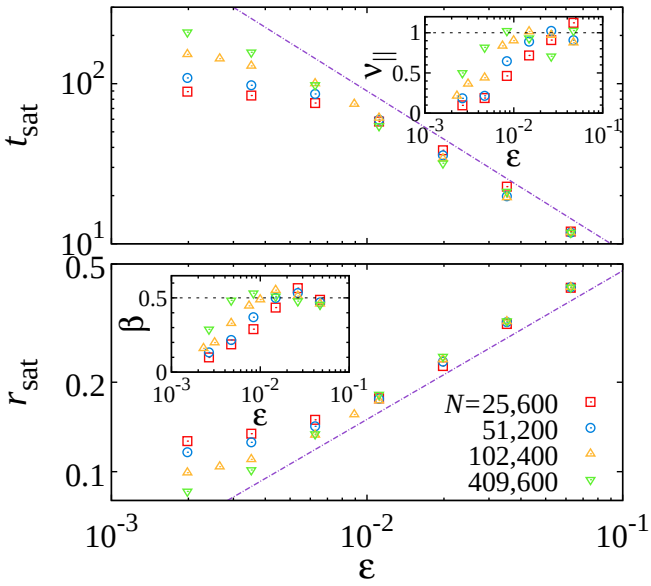

Figure 3.5: Measurement of $\nu_{\|}$ and β. The straight lines are guides for eyes and their slopes are (top)-1.0 and (bottom)0.5.

3.4.2 Starting from disordered state, $r(0) = O(N^{-1/2})$

The Randomness of initial phases makes $r(0) \sim O(N^{-1/2})$. But, the order parameters converge to a same value regardless of the initial phases in the end (See Fig. 3.6). This is a property of a continuous phase transition.

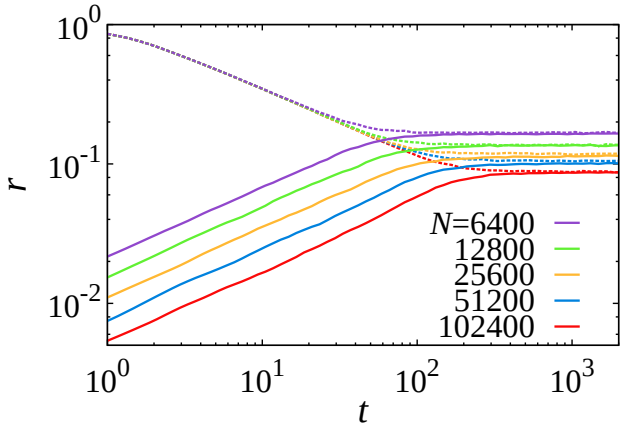

Figure 3.6: Two kinds of initial conditions are used. One is $r(0) = 1$ originated from same phases, $\phi_i(0) = \text{const}$ for all i. Another is $r(0) \approx 0$ induced from random phases in range $[0, 2\pi)$. Both initial conditions give the same value of r_{sat} at last.

Dynamic scaling relation for this case is

$$r(t, N, K_c) = N^{-\beta/\bar{\nu}} h_3(t/N^{\bar{z}}), \tag{3.3}$$

where $h_3(x) \sim$ constant for $x \gg 1$ and $h_3(x) \sim x^{\theta}$ for $x \to 0$. Considering $r_0(N) = N^{-\beta/\bar{\nu}} N^{-\bar{z}\theta} \sim N^{-1/2}$, we get $\theta = (\frac{\bar{\nu}}{2} - \beta)/\nu_{\|}$.

Another dynamic scaling form is

$$r(t, N, K_c) = N^{-1/2} t^{\theta} h_4(t/N^{\bar{z}}), \tag{3.4}$$

where $h_4(x) \sim x^{-\theta}$ for $x \gg 1$ and $h_4(x) \sim$ constant for $x \to 0$. Considering $r_{\text{sat}} \sim N^{-\beta/\bar{\nu}}$, we obtain $-1/2 + \bar{z}\theta = -\beta/\bar{\nu}$. Hence $\theta = (\frac{1}{2} - \frac{\beta}{\bar{\nu}})\frac{1}{\bar{z}} = (\frac{1}{2} - \frac{\beta}{\bar{\nu}})\frac{\bar{\nu}}{\nu_{\|}} = (\frac{\bar{\nu}}{2} - \beta)/\nu_{\|}$. Inserting mean field solution($\bar{\nu} = \frac{5}{2}, \beta = \frac{1}{2}, \nu_{\|} = 1$) gives $\theta = \frac{3}{4}$.

The numerical results show more interesting features. In Fig. 3.7 we can

verify that each graph has a different offset value which is proportional to $O(N^{-1/2})$. This feature plays a key role for the system to behave differently compared to the system starts from coherent initial phases.

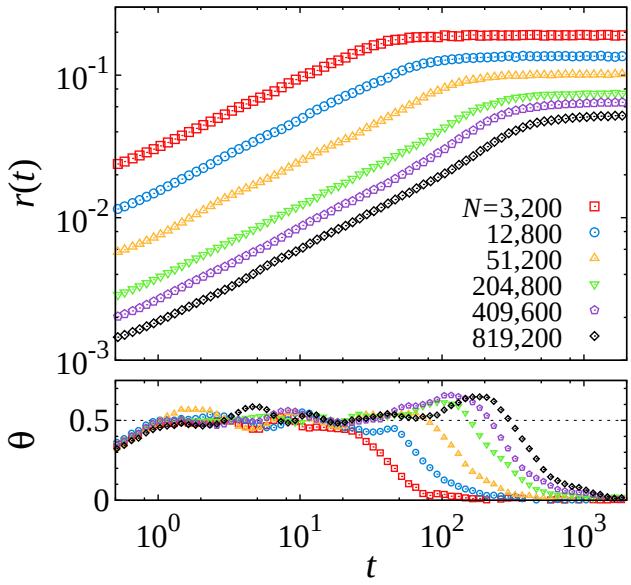

Figure 3.7: Time evolution of r at $K = K_c \approx 1.595769$ with natural frequencies chosen randomly from Gaussian distribution. The initial phases are randomly chosen from $[0, \pi)$, therefore, $r(0) \approx 0$. The number of ensemble is 1000 for $N \leq 819200$. dt=0.01 (bottom) The local slope of the main graph.

The collapsed single curve in Fig. 3.8 is dynamic scaling function h_3. The upper panel was drawn using exponents that make several curves collapse into single curve most. However, it does not reflect the real feature. The real feature is shown in the lower panel. Order parameters increase following a power-law whose exponent is 0.5 for all system sizes in early times. And then, relatively small systems about less than 10^5 saturate to their $r_{\rm sat}$. On the other hand, relatively large systems show crossover behaviors. Order parameters increase more steeply, their slopes in log-log scale are larger

than 0.5. As stated above, the slope is 3/4 in the limit of $N \to \infty$. The inset of lower panel in Fig. 3.8 is dynamic scaling function h_4.

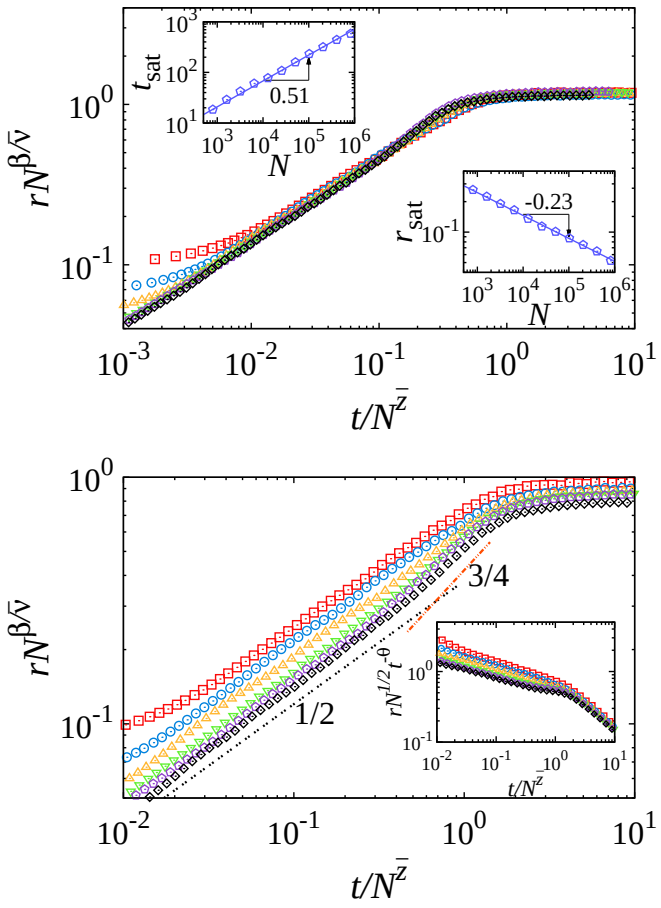

Figure 3.8: Dynamic scaling of order parameter at the criticality in case of random sampling. (top) The exponents found by the best fitting algorithm are $\beta/\bar{\nu}$=0.226, $\bar{z}$=0.512. (bottom) The theoretical values ($\beta/\bar{\nu}$=0.2, $\bar{z}$=0.4) are used.

3.5 Dynamic scaling with regular sampling

In this section, we study the effect of frequency-disorder fluctuation on the temporal behaviors of order parameter. Using Eq. (1.10), one can generate

a sequence of natural frequencies deterministically. By removing frequency-disorder fluctuation like this we can obtain only one sequence of frequencies. It is reported that the two kinds of frequency-generating methods give different values of $\bar{\nu}$. The random method gives $\bar{\nu} = 5/2$ whereas the deterministic method gives $\bar{\nu} = 5/4$ [18, 49].

3.5.1 Starting from ordered state, $r(0) = 1$

The combination of regular sampling and $r(0) = 1$ has no randomness. We don't need any ensemble average, and only the system size N decides everything. The red squares in Fig. 3.9 decays following a power law whose slope is -1/2 clearly.

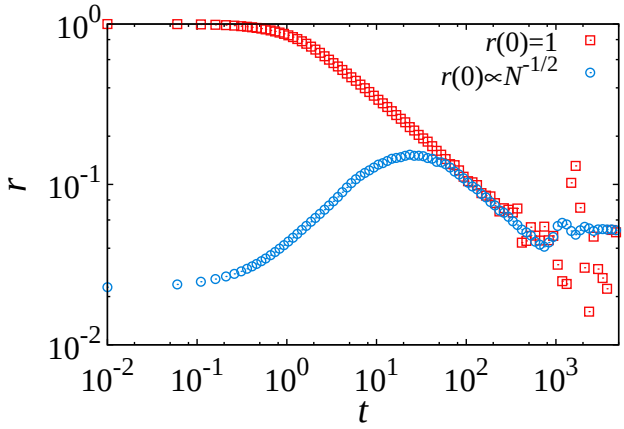

Figure 3.9: Time evolution of order parameter with regular sampling started from ordered state (red square) and disordered state (blue circle) at $K = K_c$. Fully-connected network. $N = 1600$. The number of ensemble is 1000 for blue circles and 1 for red squares.

3.5.2 Starting from disordered state, $r(0) = O(N^{-1/2})$

We found that the deterministic method makes interesting temporal behavior of $r(t)$. Starting with initial values of $\phi_i(0)$ chosen in range $[0, 2\pi)$ randomly gives $r_N(0) \sim 1/\sqrt{N}$. At first $r(t)$ increases until $t = t_{\mathrm{p1}}$ and then decreases until $t = t_{\mathrm{d1}}$ and again increases until $t = t_{\mathrm{p2}}$ and so on. In other words, $r(t)$ shows oscillating behavior as shown in Fig. 3.10.

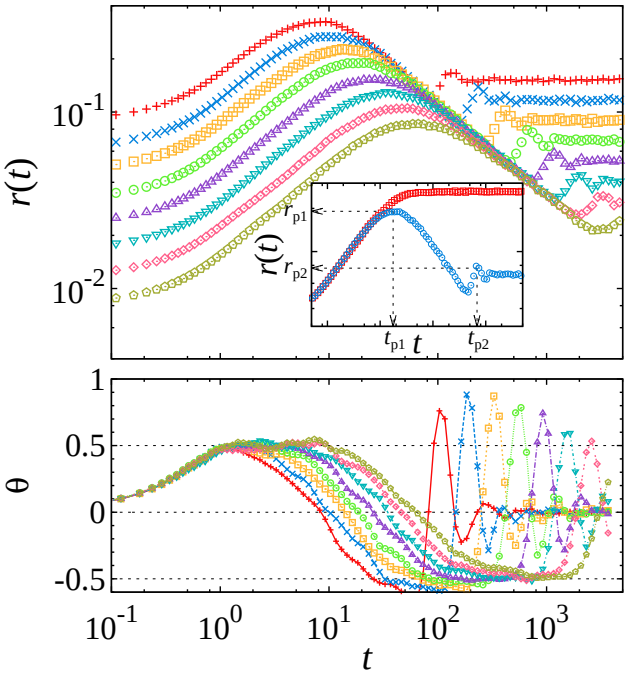

Figure 3.10: Time evolution of r at $K = K_{\mathrm{c}} \approx 1.595769$ with natural frequencies chosen regularly from Gaussian distribution. The initial phases are randomly chosen from $[0, \pi)$, therefore, $r(0) \approx N^{-1/2}$. The number of ensemble is 1000. System size N is 100, 200, 400, 800, 1600, 3200, 6400 and 12800 from top.

Let's call the first peak r_{p1} and the second peak r_{p2}. Then we can see that $r_{\mathrm{p1}} \sim N^{-\alpha_1}$ and $r_{\mathrm{p2}} \sim N^{-\alpha_2}$. And their corresponding times are $t_{\mathrm{p1}} \sim N^{\bar{z}_1}$ and $t_{\mathrm{p2}} \sim N^{\bar{z}_2}$. Two dynamic scaling relations are possible focusing

on different two regimes: $t < \tau_1$ and $t > t_{\rm p2}$.

For the first peak in r *vs.* t graph,

$$r(t, N, K_{\rm c}) = N^{-\alpha_1} f_3(t/N^{\bar{z}_1}), \tag{3.5}$$

where $\alpha_1 = 1/2 - \theta_1 \bar{z}_1$, $\theta_1 = 1/2$ and the scaling function $f_3(x) \sim$ constant for $x \gg 1$ and $f_3(x) \sim x^{\theta_1}$ for $x \to 0$.
And another scaling form is also possible:

$$r(t, N, K_{\rm c}) = N^{-1/2} t^{\theta_1} f_4(t/N^{\bar{z}_1}), \tag{3.6}$$

where $f_4(x) \sim x^{-\theta_1}$ for $x \gg 1$ and $f_4(x) \sim$ constant for $x \to 0$. Fig. 3.11 shows dynamic scaling relation of Eq. (3.5).

Now for the second peak and later in r *vs.* t graph,

$$r(t, N, K_{\rm c}) = N^{-\alpha_2} f_5(t/N^{\bar{z}_2}), \tag{3.7}$$

where $\alpha_2 = -\theta_2 \bar{z}_2$, $\theta_2 = -1/2$ and the scaling function $f_5(x) \sim$ constant for $x \gg 1$ and $f_5(x) \sim x^{\theta_2}$ for $x \to 0$.
And another scaling form is also possible:

$$r(t, N, K_{\rm c}) = t^{\theta_2} f_6(t/N^{\bar{z}_2}), \tag{3.8}$$

where $f_6(x) \sim x^{-\theta_2}$ for $x \gg 1$ and $f_6(x) \sim$ constant for $x \to 0$. In Fig. 3.12 we can see the dynamic scaling focused on the second peak and the third peak.

Another notable property of the deterministic method is that it makes

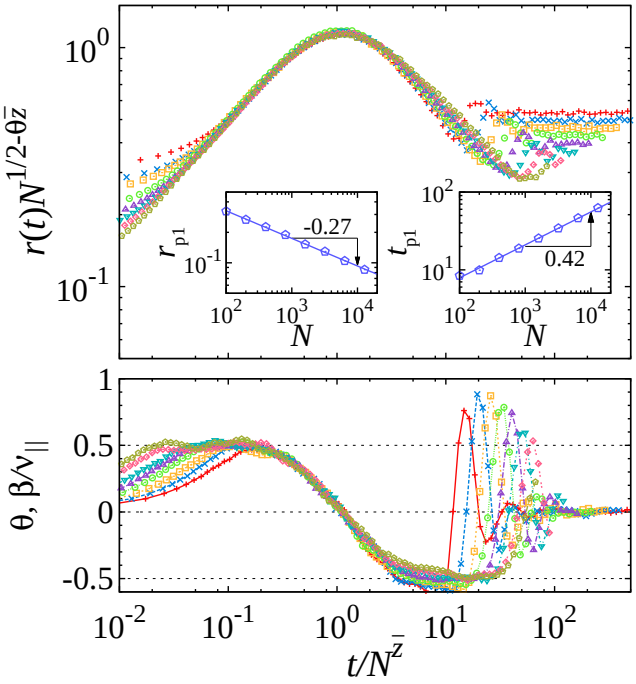

Figure 3.11: Dynamic scaling I using the first peak. The best collapsed shot. $\alpha_1 = 0.273, \bar{z}_1 = 0.424, \theta = (1/2 - \alpha_1)/\bar{z}_1 = 0.535$.

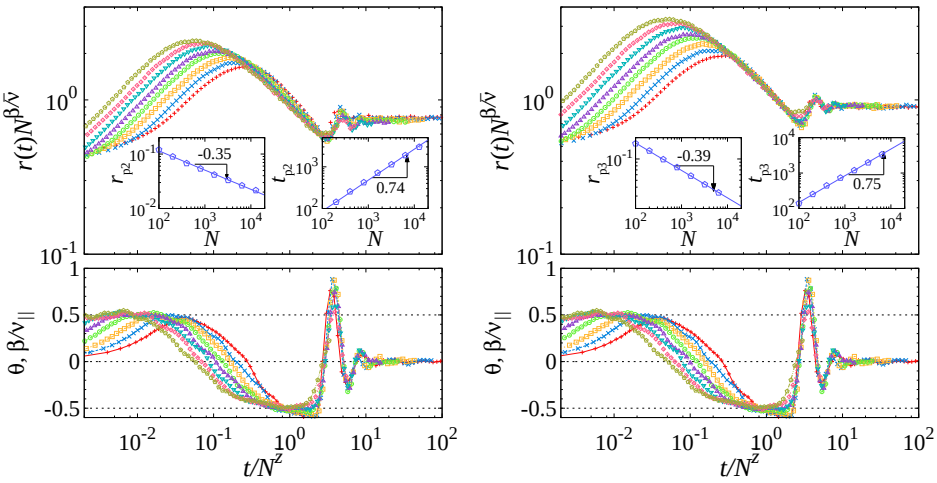

Figure 3.12: (left) Dynamic scaling II using the second peak. The best collapsed shot. $\beta/\bar{\nu} = 0.353, \bar{z} = 0.742$. (right) Dynamic scaling III using the third peak. The best collapsed shot. $\beta/\bar{\nu} = 0.387, \bar{z} = 0.753$.

saturation time, $t_{\rm sat}$ very large compare to the random method. One who wants to get the values of $r(t)$ after $t_{\rm sat}$ should, therefore, check the convergence of $r(t)$ carefully.

3.6 Dynamic scaling with thermal noise

The Kuramoto model with noise is

$$\dot{\phi}_i(t) = \omega_i + \frac{K}{N}\sum_{j=1}^{N}\sin\Big(\phi_j(t) - \phi_i(t)\Big) + \eta_i(t), \tag{3.9}$$

where $\eta_i(t)$ is a thermal noise term. Its averages are characterized as $\langle\eta_i(t)\rangle = 0$ and $\langle\eta_i(t)\eta_j(t')\rangle = 2T\delta_{ij}\delta(t-t')$.

Keeping $K = K_0 \equiv \sqrt{8/\pi}$, we increased the thermal noise strength T from 0 to 0.5 in Fig 3.13 and Fig. 3.14. As the strength of thermal noise increases, $r_{\rm sat}$ decreases. And even very weak noise ($T = 0.01$) can change the oscillating behavior of the case of regularly sampled natural frequencies. As T increases, $r_{\rm sat}$ decreases.

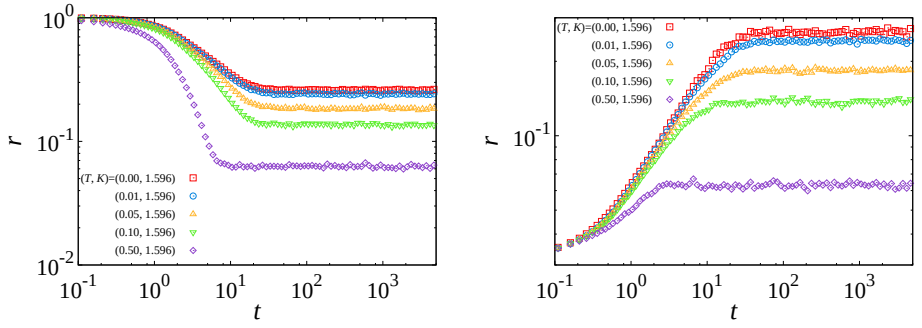

Figure 3.13: Thermal noise added. $K = K_0$, N=800, Random sampling.

The critical coupling strength $K_{\rm c}$ is a function of T and it is already

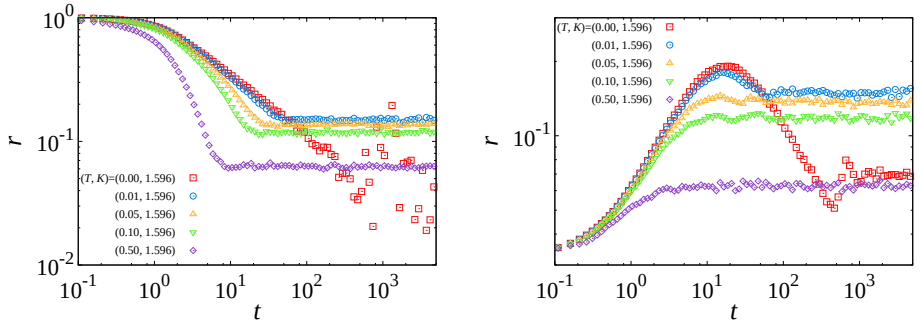

Figure 3.14: Thermal noise added. $K = K_0$, N=800, Regular sampling.

known as

$$K_{\rm c}(T) = 2 \Big/ \int_{-\infty}^{\infty} \frac{T}{T^2+\omega^2} g(\omega) {\rm d}\omega \tag{3.10}$$

in [25], [18]. By using the delta function, $\lim_{\gamma \to 0} \frac{1}{\pi} \cdot \frac{\gamma}{\gamma^2+\omega^2} = \delta(\omega)$ we obtain $K_{\rm c}(T=0) = \frac{2}{\pi g(0)}$ again. The temporal behaviors of order parameter at $K = K_{\rm c}(T)$ are plotted in Fig. 3.15 and Fig. 3.16.

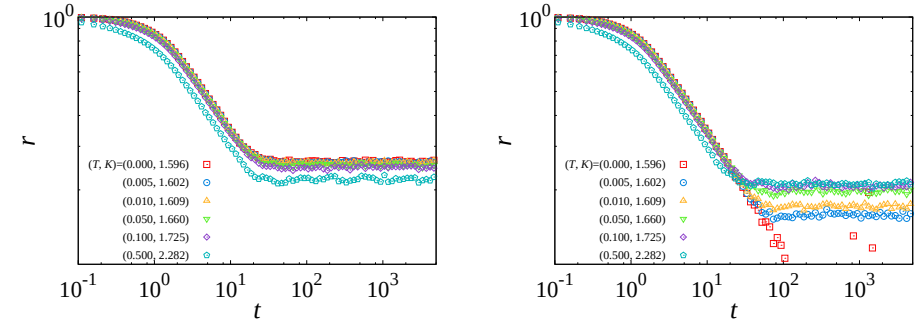

Figure 3.15: Thermal noise added. $K = K_{\rm c}(T)$, N=800, (left) Random sampling. (right) Regular sampling.

Dynamic scaling form is same to Eq. (3.3) and Eq. (3.4) except the exponents (here, $\bar{\nu} = 2, \beta/\bar{\nu} = 1/4$ and $\theta = 1/2$). See Fig. 3.17 and Fig. 3.18.

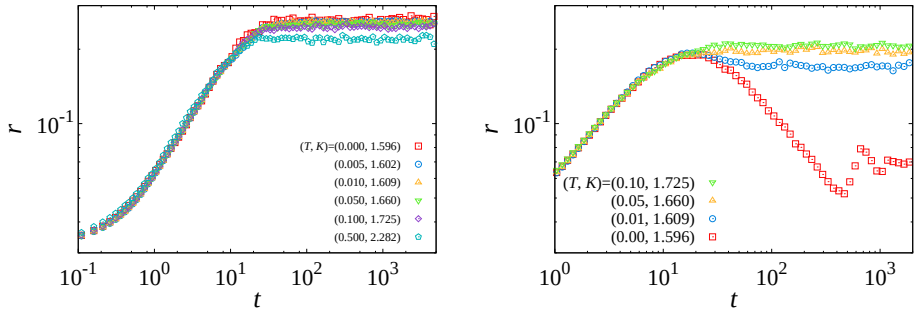

Figure 3.16: Thermal noise added. $K = K_{\mathrm{c}}(T)$, N=800, (left) Random sampling. (right) Regular sampling.

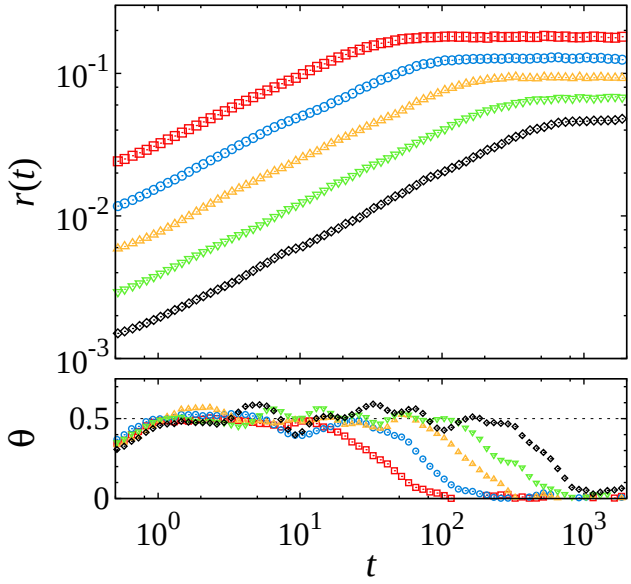

Figure 3.17: Time evolution of order parameter for Kuramoto model with noise at $K = K_{\mathrm{c}}(T = 0.1) \approx 1.725235$. Natural frequencies are chosen randomly from Gaussian distribution. The initial phases are randomly chosen from $[0, \pi)$, therefore, $r(0) \approx 0$. The number of ensemble is 1000 for $N \leq 204800$ and 500 for $N \leq 819200$. dt=0.01 (bottom)The local slope of the main graph.

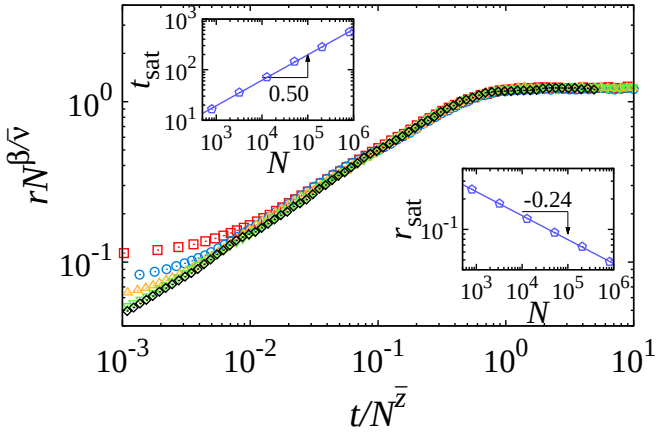

Figure 3.18: Dynamic scaling for Kuramoto model with noise. The exponents found by best fitting algorithm are $\beta/\bar{\nu}$=0.237, $\bar{z}$=0.504.

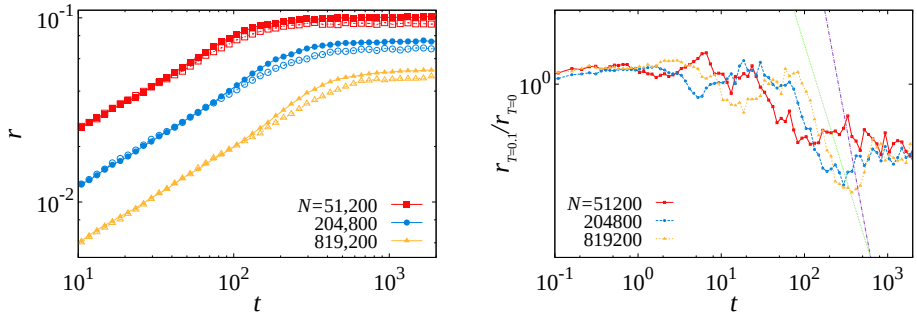

Figure 3.19: Comparison of temporal behavior of order parameter in thermal-noiseless system and thermal-noisy system. (left) r *vs.* t of thermal-noiseless system (filled symbols) at $K_c(T=0)=1.595769$. and of thermal-noisy system (open symbols) at $K_c(T=0.1)=1.725235$. (right) ratio of r with noise and r without noise.

3.7 Lattice

We also found that dynamic scaling relations exist on networks other than fully-connected network.

3.7.1 6 dimension

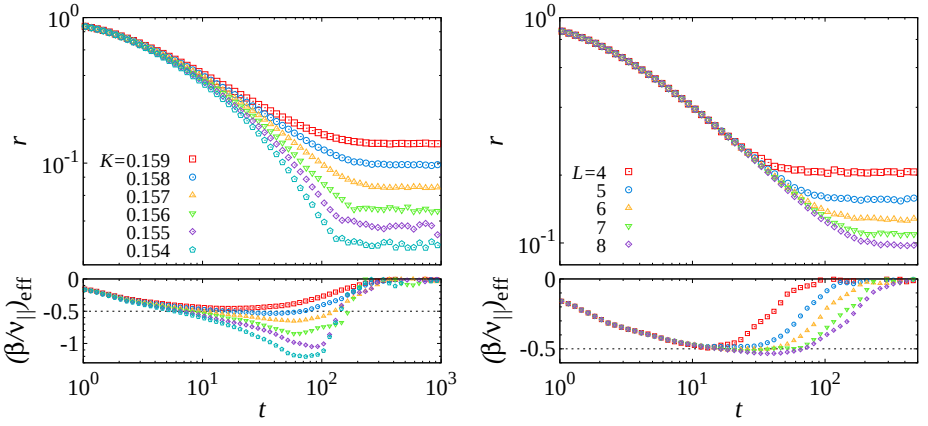

Figure 3.20: (left) Lattice d=6, time evolution of r at several K values. L=8. The number of ensemble is 500 for upper 3 graphs, 100 for lower 3 graphs. (right) Lattice d=6, time evolution of r at K=0.158 with several L. The number of ensemble is 500.

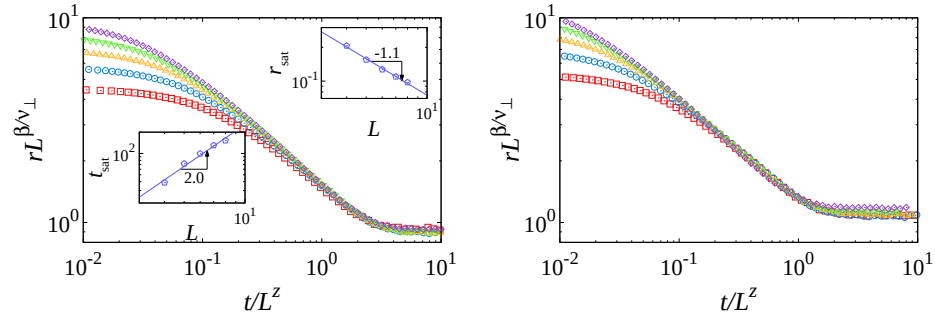

Figure 3.21: Dynamic scaling on 6 dimensional square lattice. (left) Best scaling. $\beta/\nu_\perp = 1.083, z = 1.960$, (right) $\beta/\nu_\perp = 1.2, z = 2.4$.

3.7.2 5 dimension

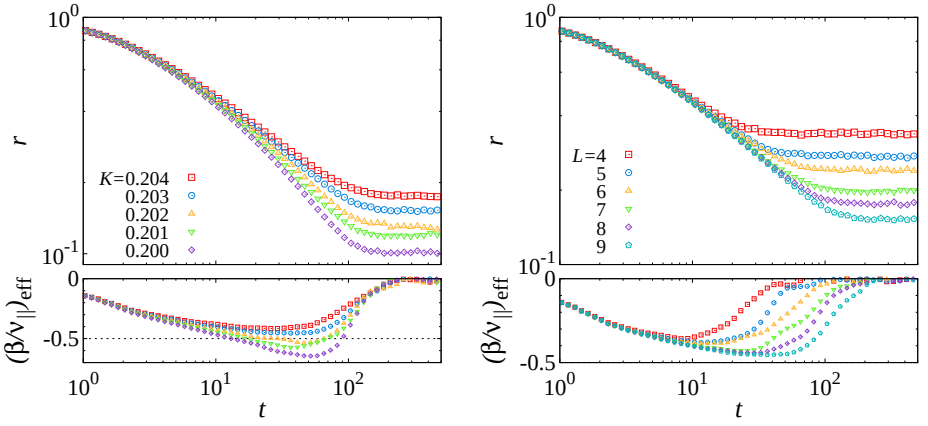

Figure 3.22: (left) Lattice d=5, time evolution of r at several K values. L=9. The number of ensemble is 500. (right) Lattice d=5, time evolution of r at K=0.203 with several L. The number of ensemble is 500.

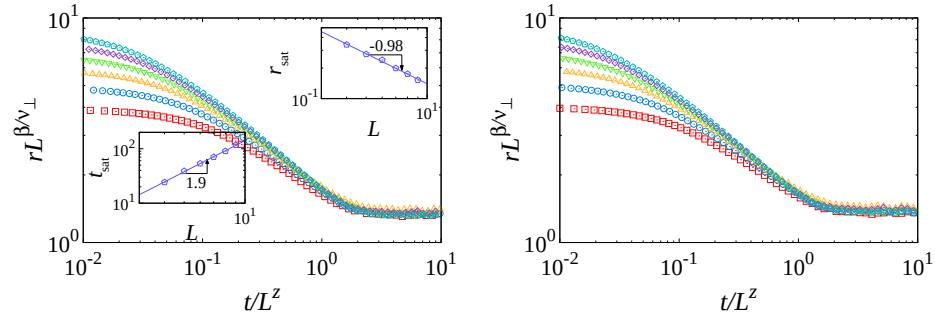

Figure 3.23: Dynamic scaling on 5 dimensional square lattice. (left) Best scaling. $\beta/\nu_\perp = 0.984, z = 1.901$, (right) $\beta/\nu_\perp = 1.0, z = 2.0$.

3.8 ER network

Classical random graphs are generated by using Gilbert's model [54]. Every pair between N vertices is connected with probability p. The mean degree $\langle k \rangle = pN = 2L/N$, where L is the number of total edges of ER network

model [55]. The graphs obtained by Gilbert's model may have two or more subgraphs. So we chose the giant component of subgraphs which has at least N vertices and then reduced the component to exact N vertices.

We set $\langle k\rangle$=16. If it would be large enough to follow the mean field solution, K_c is about $K_0\langle k\rangle/\langle k^2\rangle \approx 0.0939$, where $K_0 = \sqrt{8/\pi} \approx 1.595769$.

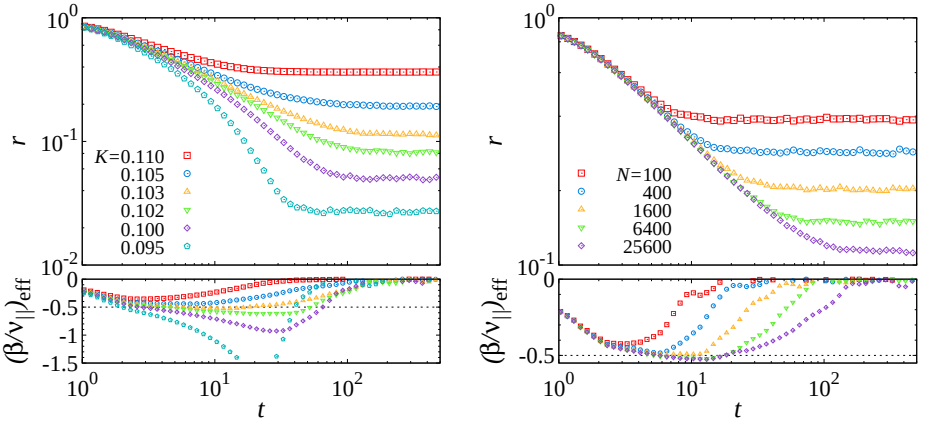

Figure 3.24: Time evolution of order parameter on ER network with $\langle k\rangle$=16. (left) at several K values with N=25600, (right) at K=0.103 with several N. The number of ensemble is 500.

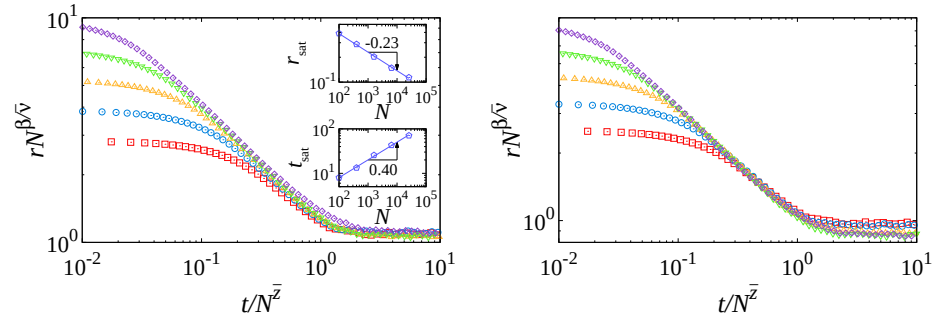

Figure 3.25: Dynamic scaling of order parameter on ER network. (left) Best scaling. $\beta/\bar{\nu} = 0.225, \bar{z} = 0.399$, (right) $\beta/\bar{\nu} = 0.2, \bar{z} = 0.4$.

Table 3.1: The results for random networks with $\langle k \rangle$=16.

	Ours	Mean Field
K_c	0.103(1)	0.094
$\beta/\bar{\nu}$	0.23(4)	0.2
$\bar{z}$	0.40(4)	0.4
$\beta/\nu_{\parallel}$	0.50(5)	0.5

3.9 Scale-free network

We generated degree sequences deterministically [56, 57] and used degree-based graph construction [58] to make SF networks.

There is a discrepancy between K_c we found and K_c in [42]. We guess they used coupling strength $K/\langle k \rangle$ or K/k_i as in [51] or [13] instead of K.

$$\begin{aligned} \langle k \rangle_{N\to\infty} &= \sum_{k=k_{\min}}^{\infty} k p(k) \\ &= \sum_{k=k_{\min}}^{\infty} k\Big(\frac{k^{-\gamma}}{\sum_{i=k_{\min}}^{\infty} i^{-\gamma}}\Big) \\ &= \frac{\zeta(\gamma-1, k_{\min})}{\zeta(\gamma, k_{\min})} \end{aligned} \tag{3.11}$$

Here $\zeta(s,q) = \sum_{k=0}^{\infty} \frac{1}{(k+q)^s}$ is Hurwitz zeta function.

$$\begin{aligned} \langle k^2 \rangle_{N\to\infty} &= \sum_{k=k_{\min}}^{\infty} k^2 p(k) \\ &= \sum_{k=k_{\min}}^{\infty} k^2\Big(\frac{k^{-\gamma}}{\sum_{i=k_{\min}}^{\infty} i^{-\gamma}}\Big) \\ &= \frac{\zeta(\gamma-2, k_{\min})}{\zeta(\gamma, k_{\min})}. \end{aligned} \tag{3.12}$$

3.9.1 γ=6.0

Here are the results for SF networks with γ=6.0.

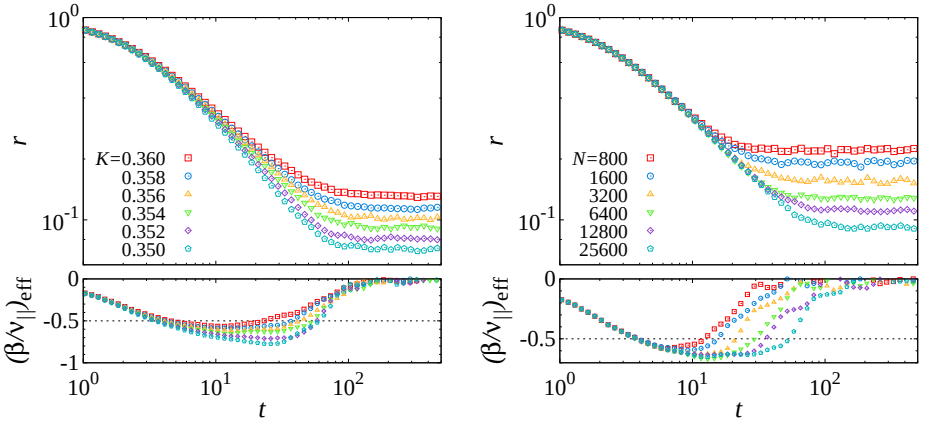

Figure 3.26: Time evolution of order parameter on SF network with $\gamma = 6.0$, $\langle k \rangle$=5.734689 ($k_{\min}$=5). The number of ensemble is 500. (left) at several K values. N=25600. (right) at K=0.354 with several N.

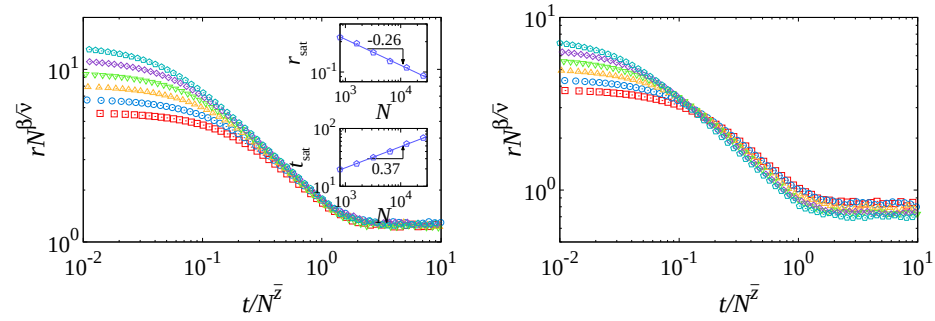

Figure 3.27: Dynamic scaling of order parameter on SF network with $\gamma = 6.0$. (left) Best scaling. $\beta/\bar{\nu} = 0.258, \bar{z} = 0.366$, (right) $\beta/\bar{\nu} = 0.2, \bar{z} = 0.4$.

3.9.2 γ=4.5

Here are the results for SF networks with γ=4.5.

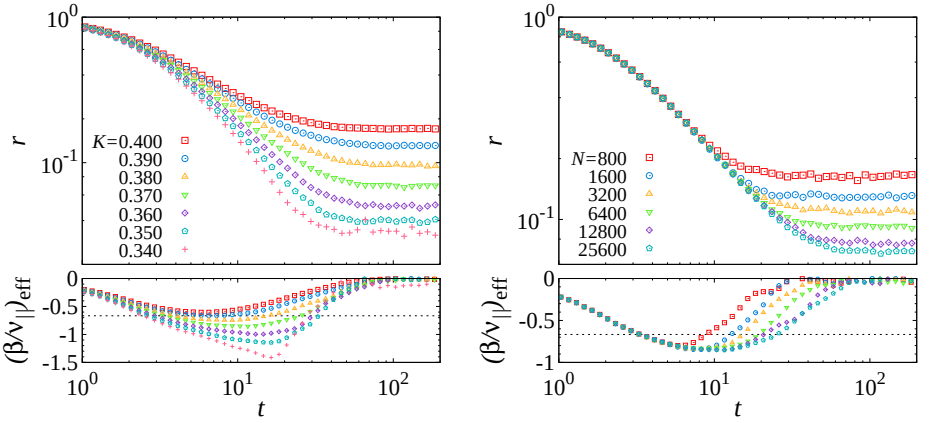

Figure 3.28: Time evolution of order parameter on SF network with $\gamma = 4.5$, $\langle k \rangle$=5.010156 ($k_{\min}$=4). The number of ensemble is 500. (left) at several K values. N=25600. (right) at K=0.37 with several N.

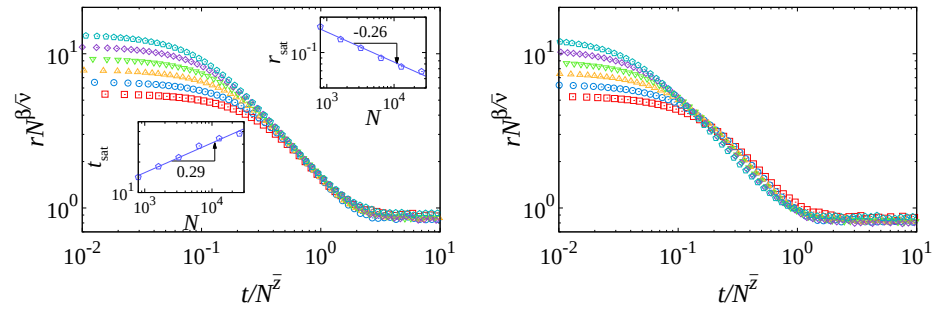

Figure 3.29: Dynamic scaling of order parameter on SF network with $\gamma = 4.5$. (left) Best scaling. $\beta/\bar{\nu} = 0.255, \bar{z} = 0.293$, (right) $\beta/\bar{\nu} = 0.25, \bar{z} = 0.375$.

3.9.3 γ=3.5

Here are the results for SF networks with γ=3.5.

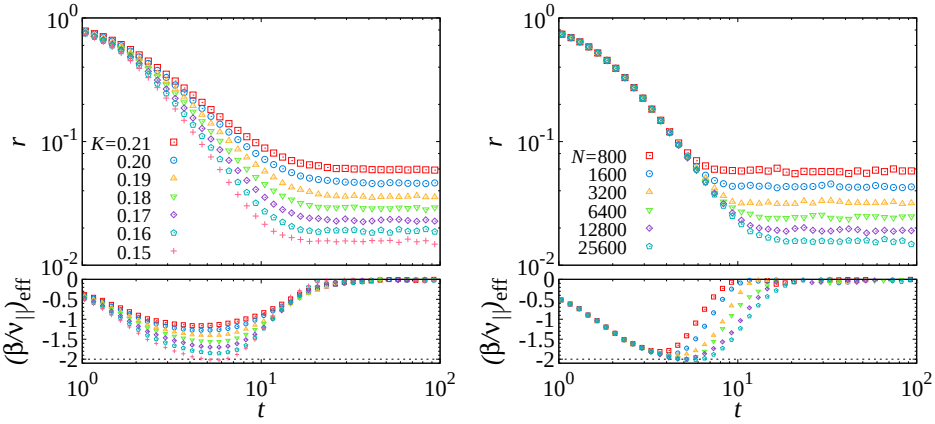

Figure 3.30: Time evolution of order parameter on SF network with $\gamma = 3.5$, $\langle k \rangle$=5.928462 ($k_{\min}$=4). The number of ensemble is 500. (left) at several K values. N=25600. (right) at K=0.15 with several N.

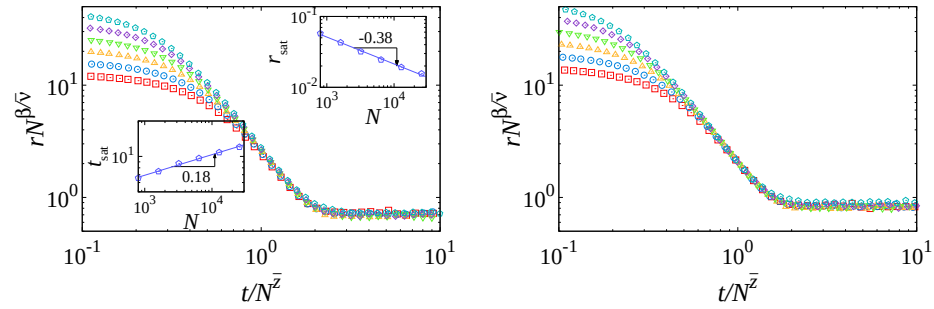

Figure 3.31: Dynamic scaling of order parameter on SF network with $\gamma = 3.5$. (left) Best scaling. $\beta/\bar{\nu} = 0.379, \bar{z} = 0.175$, (right) $\beta/\bar{\nu} = 0.4, \bar{z} = 0.2$.

Table 3.2: $\langle k \rangle$, $\langle k^2 \rangle$ and K_c of SF networks for given γ and $k_{\min}$.

$(\gamma, k_{\min})$	$\langle k \rangle_{N\to\infty}$	$\langle k^2 \rangle_{N\to\infty}$	K_c[51]	K_c[13]	K_c by us
(6.0, 5)	5.73469	34.9514	0.261828	0.261828	0.354(2)
(4.5, 4)	5.01016	29.7028	0.269168	1.34031	0.37(1)
(3.5, 4)	5.92852	62.8676	0.150484	0.819447	0.15(1)

Table 3.3: $\beta/\bar{\nu}$ and $\bar{z}$ for given γ.

γ	$\beta/\bar{\nu}(\beta,\bar{\nu})$[42]	$\beta/\bar{\nu}$ by us	$\bar{z}(=\nu_{\parallel}/\bar{\nu})$ by us
6.0	0.2(1/2, 5/2)	0.26(5)	0.37(8)
4.5	0.25(2/3, 8/3)	0.26(10)	0.29(14)
3.5	0.4(2, 5)	0.38(8)	0.18(3)

3.10 Temporal behavior of order parameter in systems exhibiting first-order phase transition

Time evolution of order parameter for the Kuramoto model with inertia is also investigated. It is known that the Kuramoto model with inertia exhibits a first-order phase transition. In that case, we found that the order parameter stays in metastable state before going to the steady state as shown in Fig. 3.32.

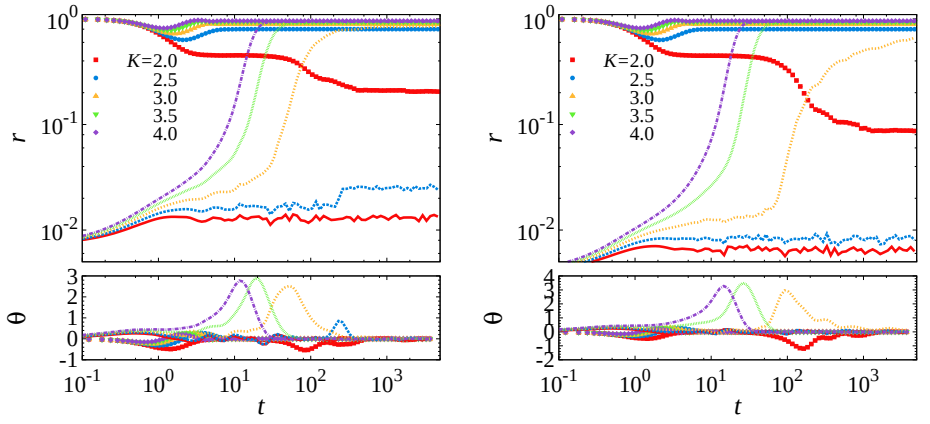

Figure 3.32: Time evolution of order parameter r, m=1, several K. (left) N=12800, (right) N=51200. The number of ensemble is 100.

3.11 Discussion

Role of disorders — Three kinds of disorders in the Kuramoto model are considered: thermal noise, sample-to-sampling fluctuation of natural frequencies $\{\omega_i\}$, and initial values $\{\phi_i(0)\}$.

- thermal noise η_i: Thermal noise is the most strong disorder among three. Regardless of existence of the other two disorders, thermal noise makes $\bar{\nu} = 2, \beta/\bar{\nu} = 1/4, \bar{z} = 1/2$.

- sample-to-sample fluctuation of natural frequencies $\{\omega_i\}$: In the absence of thermal noise, sample-to-sample fluctuation of $\{\omega_i\}$ is important. The existence of this fluctuation determines the dynamic universality class of the system and self-averageness of order parameter. Moreover, it can magic away the oscillating behaviors of order parameter which is a property of regular sampling case.

- initial value realization $\phi_i(0)$(and $\{\dot{\phi}_i(0)\}$): The fluctuation from different initial values of phase(and velocity) does not change any static exponents of dynamic exponents. It, however, determines the starting point of order parameter. Hence, the dynamic scaling function's form is affected by it.

Advantage of dynamic scaling — The existence of dynamic scaling relation at critical point is an end in itself, and besides there is another reason why it is important practically. One may want to measure order parameter for very long simulation time to find critical coupling strength, K_{c} with large system size N. But considering the computational cost of numerical integration for Eq. (1.1), there are always practical limits for system size N

or simulation time $t_{\rm sim}$. Thanks to knowledge of dynamic scaling relation, one can find $K_{\rm c}$ with short time simulation $t_{\rm sim} < t_{\rm sat}$. As shown in Fig. 3.1, the power-law behavior of $r(t)$ for $t < t_{\rm sat}$ distinguishes $K_{\rm c}$ very well. It catches the difference about $\epsilon \equiv |K/K_{\rm c} - 1| \sim 0.0025$ clearly.

3.12 Summary

In this chapter, we found the power-law decay or increase of order parameter at the criticality. And we proposed the dynamic scaling relations and confirmed the dynamic exponents both numerically and analytically. Moreover, these dynamic exponents were explained by exponents used in finite-size scaling. We tested the dynamic scaling with several combinations of three kinds of disorders. Dynamic scaling relations exist on all networks we tested: fully-connected networks, n-dimensional lattices, random (ER) networks and scale-free networks. And we confirmed that order parameter of the Kuramoto model with inertia stays in a metastable state before it is converged.

Chapter 4

Modular Synchronization and Its Application

4.1 Module detection in modular networks

A *module* on (complex) networks means a subgroup wherein the nodes are connected more densely. Modules have relatively sparse connections between each other compared to inside each module. The terms - *cluster*, *group*, *community* - have same meaning to module.

Modular structures are observed frequently in nature. For example, human brains have two hemispheres and they are connected by corpus callosum. And each hemisphere has several parts (modules) again as cerebrum, cerebellum, etc. Neural network of brain, therefore, also has modular structure. Another example is a social network. Each node in social network is a person and link connecting two nodes means that the two people has relationship. It is natural that modules exist in social network wherein nodes have more links. These modules might be any kinds of group of people like company, school, social gathering.

The Structure of complex networks, of course, is closely related with dynamics and functions of the networks [32]. It has been known that each module in human brain has its own function. Therefore it is important to understand the structures of networks including modular structure.

4.2 How to detect modular structure in modular networks?

Then how can we identify modules in modular networks? There are many *clustering* (*module-detecting*, *grouping*, *community-detecting*) *algorithms* already. Here we introduce some well-known clustering methods:

- **q-states Potts model** [59]: Initially assign spin (σ_i) states randomly. Do Monte Carlo simulation with single spin flip heat-bath algorithm and simulated annealing [60]. The modified q-state Potts Hamiltonian is

$$H = -J \sum_{(i,j)\in E} \delta_{\sigma_i,\sigma_j} + \gamma \sum_{s=1}^{q} \frac{n_s(n_s-1)}{2}. \tag{4.1}$$

- **simulated annealing(SA)** [60]: At first, each node is each module. Do simulated annealing — choose a node n_i randomly and try to move n_i to a randomly chosen neighbor module. Here, Hamiltonian is minus modularity:

$$H = -Q \equiv \sum_{\alpha} (e_{\alpha\alpha} - a_\alpha^2), \tag{4.2}$$

  where $a_\alpha = \sum_\beta e_{\alpha\beta}$, and $e_{\alpha\beta}$ is the fraction of links that connect the vertices belonging to module α and module β [61]

- **Girvan-Newman(GN)** [61, 62]: GN algorithm is an iterative divisive method based on finding and removing progressively the edges with the largest betweenness.

- **Clauset-Newman-Moore(CNM)** [63]: CNM algorithm is a hierar-

chical agglomeration algorithm developed for very large networks.

- **opinion changing rate(OCR)** [64]: OCR algorithm uses a frequency synchronization (frequency entrainment) phenomenon. Simulate the dynamics of oscillators according to

$$\dot{x}_i(t) = \omega_i + \frac{\sigma}{\sum_{i\in N_i} b_{ij}^{\alpha(t)}} \sum_{i\in N_i} b_{ij}^{\alpha(t)} \sin(x_j - x_i)\beta e^{-\beta|x_j - x_i|}. \tag{4.3}$$

  As α decreases from 0 to minus values, the groups identified based on oscillator's velocity are split into several groups. When the modularity has a maximum value, stop the process.

4.3 Modular synchronization and Kuramoto model with gauge term

There are clustering algorithms using synchronization. Examples include OCR algorithm and the method introduced in [65]. Here, we propose a new clustering algorithm related to synchronization. We introduce a modified Kuramoto model which has additional term in its sin interaction form [66]:

$$\dot{\phi}_i(t) = \omega_i - J\sum_{j=i}^{N} a_{ij} \sin\Big(\phi_i(t) - \phi_j(t) - \alpha\Big) \tag{4.4}$$

$$= \omega_i - J\sum_{j=i}^{N} a_{ij} \sin\Big(\phi_i(t) - \phi_j(t) - \eta g(B_{ij})\Big). \tag{4.5}$$

The additional term is a function of betweenness centrality. The limit of $\alpha \to 0$ obviously gives the original Kuramoto model on complex network again. In this case, the oscillators connected by links favor same phases. In a case of $\alpha = \pi$, on the other hands, they favor out of phases (The preferred

phase difference is π). We used this property to module-detecting problem. For inter-module links that are connects between two different modules, we set $\alpha_{ij} \approx \pi$. For intra-module links that are connects within same module, we set $\alpha_{ij} \approx 0$. Then oscillators within each module are synchronized separately, whereas the whole network is not synchronized globally. To assign quantitative values to α_{ij}, we define α_{ij} as $\alpha_{ij} \equiv \eta g(b_{ij}) \equiv \eta\pi \frac{b_{ij}-b_{\min}}{b_{\max}-b_{\min}}$. Here b_{ij} is the *link betweenness centrality* which is a fraction of the shortest paths crossing the link L_{ij} among all shortest paths between all possible pairs of nodes. This quantity can be thought as an indicator for the loads burdened on the link L_{ij}.

For test bed network, we use *ad hoc* network [67] drawn in Fig. 4.1.

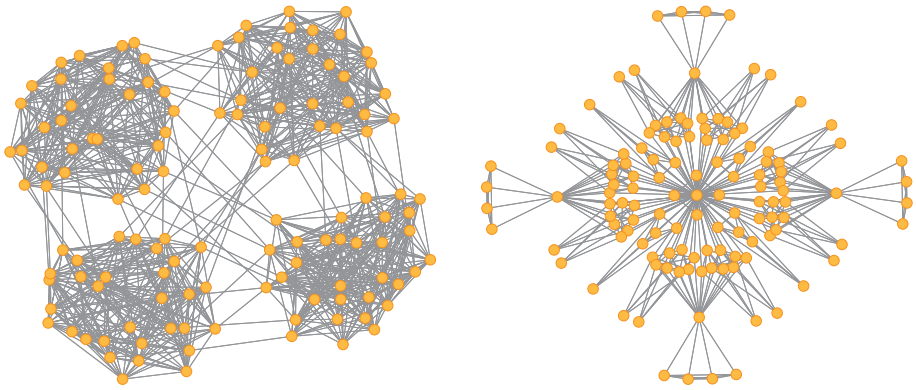

Figure 4.1: (left) *ad hoc* network with 4 groups. Each group has 32 nodes. $z_{\text{out}} = 0.05$. (right) hierarchical network with 3 levels and 125 nodes.

The *ad hoc* network has four modules and each module is composed of 32 nodes. The average degree (the number of neighbors) $\langle k \rangle$ is 16. Gaussian distribution with zero mean and unit variance is used for the natural frequency ($\{\omega_i\}$) sampling.

Before going further, we tested the idea is working with a hierarchical

network [68]. Fig. 4.2 is a dendrogram for hierarchical network drawn based on Eq. (4.5) and phase similarity $C_{ij} \equiv \left[\left\langle \left(1+\cos\left(\phi_i(t)-\phi_j(t)\right)\right)/2 \right\rangle\right]$.

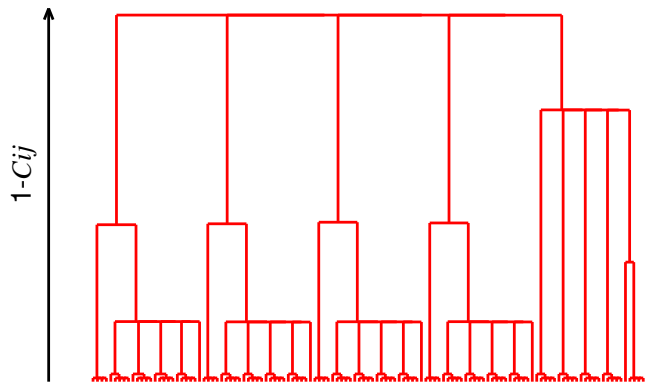

Figure 4.2: The dendrogram based on the phase similarity between connected pairs of vertices for the hierarchical network with three levels.

4.4 Clustering algorithm

Here we propose a new clustering algorithm using modular synchronization.

(step 1) Calculate Eq. (4.5) for all oscillators with a sufficiently large coupling constant J. Obtain each oscillator's phase, $\{\phi_i(t)\}$ in the steady state.

(step 2) Measure the phase similarity, $C_{ij} \equiv \left[\left\langle \frac{1+\cos\left(\phi_i(t)-\phi_j(t)\right)}{2} \right\rangle\right]$ for all link L_{ij} (pair of connected oscillators (i,j)). Here, $\langle\cdots\rangle$ means average over times and $[\cdots]$ represents average over different initial configurations $\{\omega_i\}$ and initial random phases $\{\phi_i(0)\}$.

(step 3) Starting from all nodes and no links, add a link L_{ij} in descending order of measured C_{ij}.

(step 4) Repeat the step 3 until the modularity Q becomes maximum. The modularity Q is defined as

$$Q \equiv \sum_{\alpha} (e_{\alpha\alpha} - a_{\alpha}^2), \tag{4.6}$$

where $a_\alpha = \sum_\beta e_{\alpha\beta}$, and $e_{\alpha\beta}$ is the fraction of links that connect the vertices belonging to module α and module β[61].

Connected nodes after this process are regarded as modules. The links that existed originally, but not connected yet are regarded as inter-modular links.

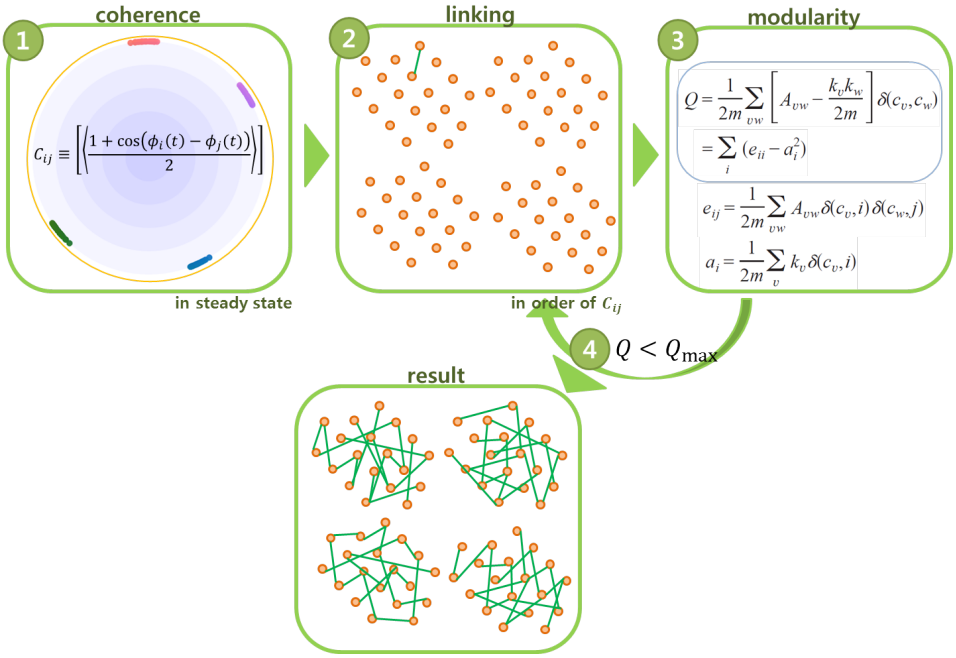

Figure 4.3: Clustering algorithm using modified Kuramoto model.

4.5 Numerical results

We measured *group phase* which is a mean phase of 32 nodes within a same group (module) in Fig. 4.4. The group phase varies with time and goes to the different value with each other in the end. And we can see that oscillators in a module are synchronized but whole oscillators in a network are not synchronized in Fig. 4.5.

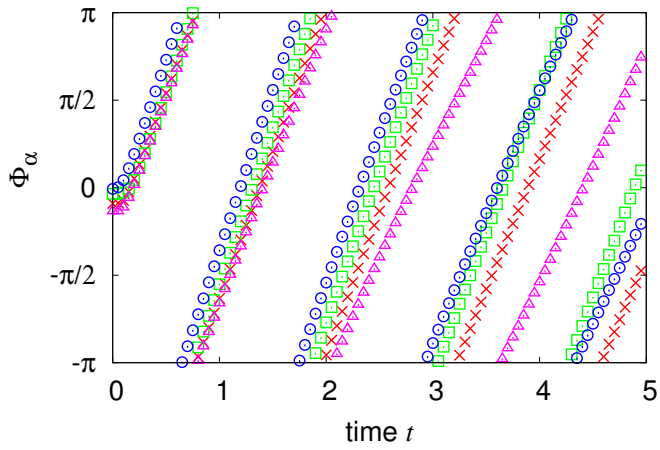

Figure 4.4: The time evolution of average phases of the four modules, distinguished by different symbols, for the *ad hoc* network with $z_{\text{out}}/\langle k\rangle = 0.05$ when $\eta = 1.0$ and $J = 2.0$.

As an indicator for performance of each clustering algorithms, we used *mutual information*, $I(A,B)$ [67]

$$I(A,B) = \frac{-2\sum_{i=1}^{M}\sum_{j=1}^{M'}\log(\frac{N_i^j}{N_i N^j})}{\sum_{i=1}^{M} N_i \log(\frac{N_i}{N}) + \sum_{j=1}^{M'} N^j \log(\frac{N^j}{N})}, \tag{4.7}$$

where $M = 4$ is the number of preassigned modules and M' is the number of detected modules. N_i^j is the number of vertices belonging to the ith preassigned and the jth detected modules, $N_i = \sum_j N_i^j$ and $N^j = \sum_i N_i^j$.

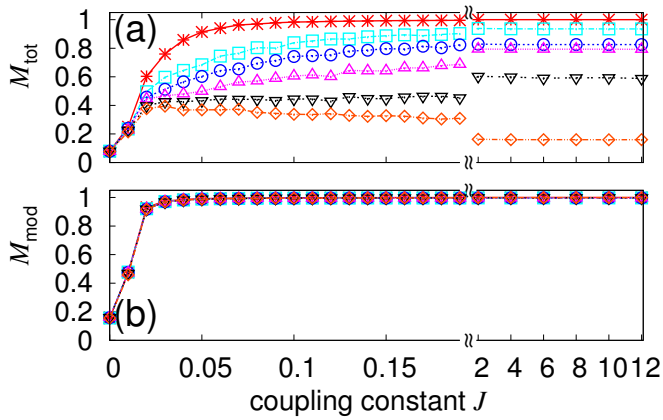

Figure 4.5: The order parameter defined over the entire network (a) and within a module (b) versus the coupling constant J for the *ad hoc* network in case of $z_{\rm out}/\langle k\rangle = 0.05$. Data are for $\eta = 0.0$, 0.6, 0.7, 0.8, 0.9 and 1.0 from the top in (a). The same symbols are used for (b), but data for different η collapse onto the single curve.

In Fig. 4.6 we plotted $I(A,B)$ *vs.* $z_{\rm out}/\langle k\rangle$ for several kinds of clustering methods including our method. Our method shows quite good performance which is comparable to GN algorithm practically. Our method does not

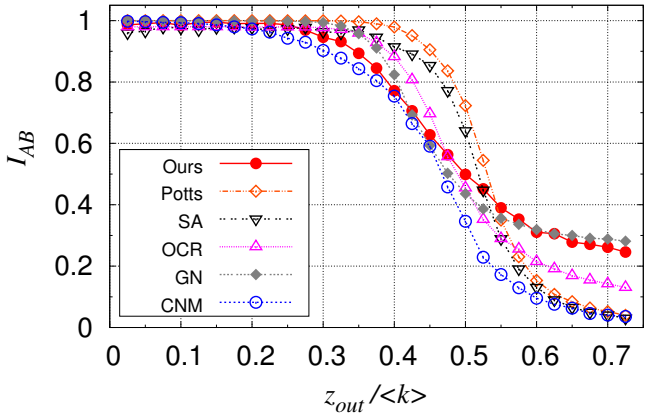

Figure 4.6: The mutual information versus $z_{\rm out}/\langle k\rangle$, the fraction of inter-modular edges per mean degree for the *ad hoc* network.

need to tuning any parameter and computational cost is $O(NL)$ which is a relatively low cost comparing the others. See the details in Table 4.1. Because our method determines the number of clusters based on modularity Q, it also has a resolution limit of modularity discovered by [69].

Table 4.1: Computational costs and characteristics of clustering algorithms.

Method	Cost	Ensemble	Parameter tuning	Etc.
Ours	$O(NL)$	required	no parameters	-
Potts	parameter dependent	required	required	-
SA	-	required	-	-
OCR	$O(NL)$	required	required	-
GN	$O(NL^2)$	no	no parameters	-
CNM	$O(N \ln^2 N)$	-	no parameters	large N

4.6 Summary

We introduced an additional term in the interaction function of the Kuramoto model. The term is a function of the link betweenness centrality. Because of its effects, each module in modular networks synchronizes but the whole network desynchronizes. This feature enables us to find modular structure of given complex networks.

Chapter 5

Conclusion

In this dissertation, we have studied synchronization of coupled oscillators. Synchronization is one of the most popular phenomena among collective behaviors of many-body systems. The Kuramoto model describes phase synchronization dynamics with coupled differential equations having an interaction term.

The most of previous studies discarded order parameter data obtained before the system goes to the steady state. We focused the early-time order parameter data and find its interesting behaviors. One is a power-law decay or increase of order parameter at the critical coupling strength. Based on the time evolution of order parameter following a power-law, we conjectured dynamic scaling relation for several combinations of three disorders. The disorders include thermal noise, sample-to-sample fluctuation of natural frequencies, and initial phase configurations. The dynamic exponents used in dynamic scaling form can be derived from the static exponents used in finite-size scaling theory. And it was confirmed by numerical simulations.

We discovered that random sampling and regular sampling for natural frequencies show different behaviors and they belong to different dynamic universality classes. Especially, we found the true scaling regime for a case of random sampling. It is hard to find true scaling regime with small system sizes. The systems whose sizes are at least $N = O(10^5)$ show crossover in order parameter *vs.* time graphs. And for regular sampling case, the or-

der parameter oscillates and converges very slowly. This damped oscillation of order parameter is a totally new phenomenon not discovered in synchronization problem yet. Moreover, we confirmed that the dynamic scaling relations exist in all kinds of networks: Fully-connected networks, n-dimensional square lattice, ER network and SF network are tested as a structure of oscillators. One can locate the critical coupling strength using dynamic scaling relation on complex networks. Besides, through the temporal behavior of order parameter, we verified the existence of metastable state for Kuramoto model with inertia. Therefore, one can identify the phase transition type by study the temporal behavior of order parameter.

We applied synchronization phenomenon to clustering problem. By modifying interaction term of the Kuramoto model, we identified modular structures of given networks successfully. Using link-betweenness centrality is a key to induce phase difference between two other clusters. Our algorithm shows similar performance to other algorithms and has advantages of light computational cost, $O(NL)$ and no parameter tuning.

Appendices

Appendix A

Numerical Simulation Method

A.1 Kahan's summation

A value obtained from iterative numerical summation has an accumulative error. This error comes from floating-point precision and increases as the number of iteration grows. Usually the error is proportional to the number of iterations. Kahan's summation method [70] reduces the accumulative numerical error by introducing error-canceling term in a summation loop. For a floating-point error generated in the nth iteration, the summation value is compensated in the $n+1$th step. Then, no matter how much iteration is calculated, the total error only depends on single floating-point precision. The pseudocode for the algorithm is [71] like below:

Algorithm 1 Kahan's summation algorithm

```
procedure KahanSum(input)
    var sum ← 0.0
    var c ← 0.0
    for i ← 1, input.length do
        var y ← input[i] − c
        var t ← sum + y
        c ← (t − sum) − y
        sum ← t
    return sum
```

A.2 Computational cost: running time

Performing numerical simulation with computers, we have some limits in CPU power, memory and time. Therefore, estimating computational cost for given system size and iteration number before we start numerical simulations is important. Kuramoto model (Eq. (1.1)) is composed of N coupled differential equations. Each of them requires N iterations to calculate its interaction term. The CPU time, therefore, is proportional to $O(N^2)$ — As system size N increases, the CPU time increases more rapidly in power law $O(N^2)$. It is a very unfavorable situation. Using Eq. (2.17), however, can reduce the simulation time drastically. We just calculate the order parameter once and use the same value in N interaction terms. The CPU time, therefore, is proportional to system size linearly, $O(N)$. This is the story of fully-connected networks. Using other complex networks instead of fully-connected networks makes the computational cost $O(N^2)$ again.

A.3 How to determine r_{sat} and t_{sat}

It is a subtle task to pinpoint a saturation point (t_{sat}, r_{sat}) exactly on r *vs.* t graph. The most unsatisfying method to do this may be peaking up the point with eyes manually(using mouse point on monitor screen or a pencil on printed paper). Its results may depend on who analyzes the data and when the analysis is performed. We, therefore, need more systematic and autonomous methods.

The method used in this study is described below:

1. We have data set from which we can plot r *vs.* t graph. This is, of course, ensemble-averaged data set.

2. By performing moving-average, make the graph smooth. And calculate successive slope, $r'(t)$ of the graph.

3. Fix some small value, $\epsilon_r > 0$ and find the smallest t_{1r} such that $|r'(t)| < \epsilon_r$ for $t > t_{1r}$. Average all successive points their time $t > t_{1r}$ to get r_{sat}. (If you are working with log-periodic time data, calculate a weighted average value.)

4. Fix some value, $\epsilon_t > 0$. Find the largest t_{1t} such that $|r'(t)| < \epsilon_t$ for $t < t_{1t}$ and the smallest t_{2t} such that $|r'(t)| < \epsilon_t$ for $t > t_{2t}$. Fit the data whose time t are between t_{1t} and t_{2t} as $y = ax + b$ using linear regression. This straight line and $y = r_{\text{sat}}$ meet at one point that gives t_{sat}.

There might be several algorithms other than this method. Most of them might give similar results with consistency within error range if they are not too peculiar methods. Whatever method you choose among them, it is important to use only one systematic method for every data set.

Appendix B

σ/K and time step $\mathrm{d}t$

Let's start from Kuramoto model,

$$\dot{\phi}_i = \omega_i + \frac{K}{N}\sum_{j=1}^{N}\sin(\phi_j - \phi_i). \tag{B.1}$$

Assume that The variance of natural frequency distribution is σ^2. And applying a new time scale, $\mathrm{d}t' = \sigma \mathrm{d}t$ to Eq. (B.1) gives,

$$\begin{aligned} \dot{\phi}_i &= \omega_i/\sigma + \frac{K/\sigma}{N}\sum_{j=1}^{N}\sin(\phi_j - \phi_i) && \text{(B.2)} \\ &= \omega_i' + \frac{K'}{N}\sum_{j=1}^{N}\sin(\phi_j - \phi_i). && \text{(B.3)} \end{aligned}$$

Now, the distribution function of natural frequencies in Eq. (B.3) has an unit variance. Note that ω_i'/K' in Eq. (B.3) is equal to ω_i/K in Eq. (B.1). This means that natural frequencies with small (large) variance need small (large) coupling strength. In other words, if we keep the ratio of σ and K, the dynamics of system are equal, therefore we get same order parameter r. If σ is large (small), $\mathrm{d}t(=\mathrm{d}t'/\sigma)$ is smaller (larger) than $\mathrm{d}t'$ which means large (small) variance needs more dense (sparse) time step.

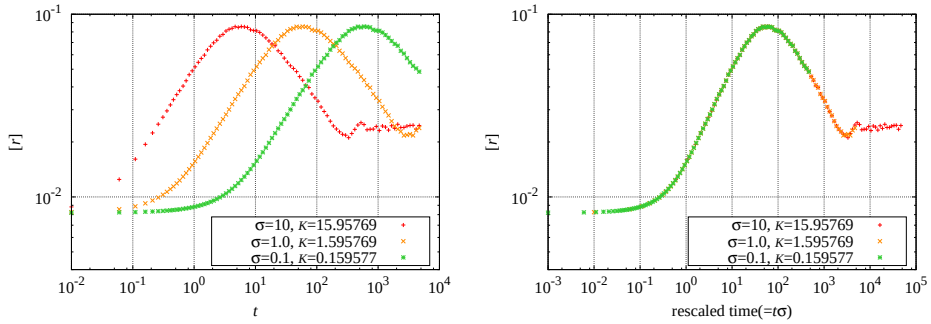

Figure B.1: $[r]$ *vs.* t for several cases with same K/σ. Fully-connected network, N=12800, regular sampling, $r(0) = O(N^{-1/2})$, The number of ensemble is 500. $(\sigma, K) = 10(\sigma_0, K_0), (\sigma_0, K_0), 0.1(\sigma_0, K_0)$ where $(\sigma_0, K_0) = (1.0, 1.595769)$. The curves in the left figure are collapsed well in the right figure. We used dt=0.01 for all cases, but it is good to adjust dt for fairer comparison. dt should be inversely proportional to σ.

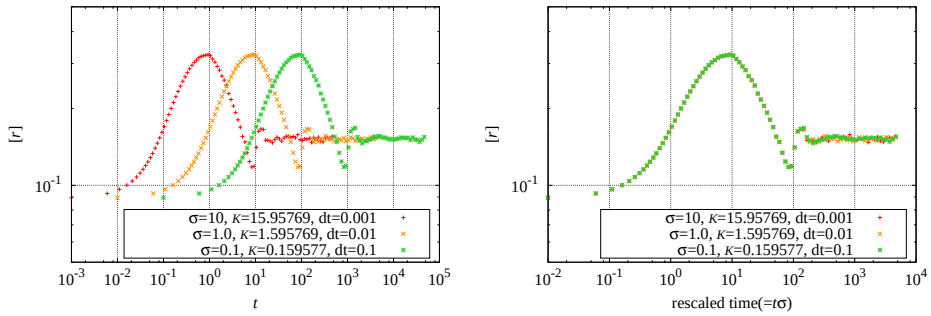

Figure B.2: $[r]$ *vs.* t for several cases with same K/σ but different dt, Fully-connected network, N=100, regular sampling, $r(0) = O(N^{-1/2})$, The number of ensemble is 1000. $(\sigma, K, \mathrm{d}t) = (10\sigma_0, 10K_0, 0.1\mathrm{d}t_0), (\sigma_0, K_0, \mathrm{d}t_0), (0.1\sigma_0, 0.1K_0, 10\mathrm{d}t_0)$ where $(\sigma_0, K_0, \mathrm{d}t_0) = (1.0, 1.595769, 0.01)$. The curves in the left figure are collapsed well in the right figure.

Bibliography

[1] S. Boccaletti, *The Synchronized Dynamics of Complex Systems*, edited by A. C. Luo and G. Zaslavsky, Monograph Series on Nonlinear Science and Complexity, Vol. 6 (Elsevier Science, 2008).

[2] Wikipedia, "Christiaan huygens," `http://en.wikipedia.org/wiki/Christiaan_Huygens` (2013).

[3] S. H. Strogatz, *Sync: The Emerging Science of Spontaneous Order* (Hyperion Books, 2003).

[4] M. Rohden, A. Sorge, M. Timme, and D. Witthaut, Phys. Rev. Lett. **109**, 064101 (2012).

[5] G. Saxena, A. Prasad, and R. Ramaswamy, Physics Reports **521**, 205 (2012).

[6] D. V. Ramana Reddy, A. Sen, and G. L. Johnston, Phys. Rev. Lett. **80**, 5109 (1998).

[7] Y. Kuramoto, in *International Symposium on Mathematical Problems in Theoretical Physics*, Lecture Notes in Physics, Vol. 39, edited by H. Araki (Springer Berlin Heidelberg, 1975) pp. 420–422.

[8] Y. Kuramoto, *Chemical Oscillations, Waves and Turbulence* (Springer-Verlag, Berlin, 1984).

[9] Y. Kuramoto and I. Nishikawa, J. Stat. Phys. **49**, 569 (1987).

[10] S. H. Strogatz, Physica D **143**, 1 (2000).

[11] J. A. Acebrón, L. L. Bonilla, C. J. Pérez Vicente, F. Ritort, and R. Spigler, Rev. Mod. Phys. **77**, 137 (2005).

[12] J. Gómez-Gardeñes, Y. Moreno, and A. Arenas, Phys. Rev. Lett. **98**, 034101 (2007).

[13] E. Oh, D.-S. Lee, B. Kahng, and D. Kim, Phys. Rev. E **75**, 011104 (2007).

[14] D. Pazó, Phys. Rev. E **72**, 046211 (2005).

[15] L. Bonilla, J. Neu, and R. Spigler, Journal of Statistical Physics **67**, 313 (1992).

[16] J. A. Acebrón, L. L. Bonilla, and R. Spigler, Phys. Rev. E **62**, 3437 (2000).

[17] Wikipedia, "Mersenne twister," `http://en.wikipedia.org/wiki/Mersenne_twister` (2013).

[18] S.-W. Son and H. Hong, Phys. Rev. E **81**, 061125 (2010).

[19] H.-A. Tanaka, A. J. Lichtenberg, and S. Oishi, Phys. Rev. Lett. **78**, 2104 (1997).

[20] A.-L. Barabási and H. E. Stanley, *Fractal Concepts in Surface Growth* (Cambridge University Press, Cambridge, 1995).

[21] H. Hong, H. Park, and M. Y. Choi, Phys. Rev. E **72**, 036217 (2005).

[22] H. Hong, H. Park, and L.-H. Tang, Journal of the Korean Physical Society **49**, L1885 (2006).

[23] K. Binder, K. Vollmayr, H.-P. Deutsch, J. D. Reger, M. Scheucher, and D. P. Landau, International Journal of Modern Physics C **3**, 1025 (1992).

[24] K. Vollmayr, J. Reger, M. Scheucher, and K. Binder, Zeitschrift für Physik B Condensed Matter **91**, 113 (1993).

[25] H. Sakaguchi, Progress of Theoretical Physics **79**, 39 (1988).

[26] M. Y. Choi, Y. W. Kim, and D. C. Hong, Phys. Rev. E **49**, 3825 (1994).

[27] H.-A. Tanaka, A. J. Lichtenberg, and S. Oishi, Physica D: Nonlinear Phenomena **100**, 279 (1997).

[28] H. Hong, M. Y. Choi, J. Yi, and K.-S. Soh, Phys. Rev. E **59**, 353 (1999).

[29] H. Hong, H. Park, and M. Y. Choi, Phys. Rev. E **70**, 045204 (2004).

[30] H. Hong, H. Chaté, H. Park, and L.-H. Tang, Phys. Rev. Lett. **99**, 184101 (2007).

[31] J. Gómez-Gardeñes, Y. Moreno, and A. Arenas, Phys. Rev. E **75**, 066106 (2007).

[32] M. Newman, SIAM Review **45**, 167 (2003).

[33] J. Gómez-Gardeñes, S. Gómez, A. Arenas, and Y. Moreno, Phys. Rev. Lett. **106**, 128701 (2011).

[34] T. K. D. Peron and F. A. Rodrigues, Phys. Rev. E **86**, 056108 (2012).

[35] B. C. Coutinho, A. V. Goltsev, S. N. Dorogovtsev, and J. F. F. Mendes, Phys. Rev. E **87**, 032106 (2013).

[36] H. Hong, M. Y. Choi, B.-G. Yoon, K. Park, and K.-S. Soh, Journal of Physics A: Mathematical and General **32**, L9 (1999).

[37] H. Hong and M. Y. Choi, Phys. Rev. E **62**, 6462 (2000).

[38] H. Hong, G. S. Jeon, and M. Y. Choi, Phys. Rev. E **65**, 026208 (2002).

[39] D. Taylor, E. Ott, and J. G. Restrepo, Phys. Rev. E **81**, 046214 (2010).

[40] Y. Moreno and A. F. Pacheco, EPL (Europhysics Letters) **68**, 603 (2004).

[41] T. Ichinomiya, Phys. Rev. E **70**, 026116 (2004).

[42] H. Hong, H. Park, and L.-H. Tang, Phys. Rev. E **76**, 066104 (2007).

[43] H. Khoshbakht, F. Shahbazi, and K. A. Samani, Journal of Statistical Mechanics: Theory and Experiment **2008**, P10020 (2008).

[44] D. Stauffer and A. Aharony, *Introduction To Percolation Theory*, 2nd ed. (Taylor & Francis, London, 1994).

[45] H. Daido, Journal of Statistical Physics **60**, 753 (1990).

[46] S. Wiseman and E. Domany, Phys. Rev. E **52**, 3469 (1995).

[47] A. Aharony and A. B. Harris, Phys. Rev. Lett. **77**, 3700 (1996).

[48] S. Wiseman and E. Domany, Phys. Rev. Lett. **81**, 22 (1998).

[49] L.-H. Tang, J. Stat. Mech. , P01034 (2011).

[50] H. Daido, Journal of Physics A: Mathematical and General **20**, L629 (1987).

[51] D.-S. Lee, Phys. Rev. E **72**, 026208 (2005).

[52] S. H. Strogatz and R. E. Mirollo, J. Stat. Phys. **63**, 613 (1991).

[53] S.-W. Son, H. Jeong, and H. Hong, Phys. Rev. E **78**, 016106 (2008).

[54] E. N. Gilbert, The Annals of Mathematical Statistics **30**, 1141 (1959).

[55] P. Erdős and A. Rényi, Publ. Math. Debrecen **6**, 290 (1959).

[56] J. D. Noh and H. Park, Phys. Rev. E **79**, 056115 (2009).

[57] S. H. Lee, M. Ha, H. Jeong, J. D. Noh, and H. Park, Phys. Rev. E **80**, 051127 (2009).

[58] H. Kim, Z. Toroczkai, P. L. Erdos, I. Miklos, and L. A. Szekely, J. Phys. A: Math. Theor. **42**, 392001 (2009).

[59] J. Reichardt and S. Bornholdt, Phys. Rev. Lett. **93**, 218701 (2004).

[60] S. Kirkpatrick, C. D. Gelatt, and M. P. Vecchi, Science **220**, 671 (1983).

[61] M. E. J. Newman and M. Girvan, Phys. Rev. E **69**, 026113 (2004).

[62] M. Girvan and M. E. J. Newman, Proceedings of the National Academy of Sciences **99**, 7821 (2002).

[63] A. Clauset, M. E. J. Newman, and C. Moore, Phys. Rev. E **70**, 066111 (2004).

[64] S. Boccaletti, M. Ivanchenko, V. Latora, A. Pluchino, and A. Rapisarda, Phys. Rev. E **75**, 045102 (2007).

[65] A. Arenas, A. Díaz-Guilera, and C. J. Pérez-Vicente, Phys. Rev. Lett. **96**, 114102 (2006).

[66] E. Oh, C. Choi, B. Kahng, and D. Kim, EPL (Europhysics Letters) **83**, 68003 (2008).

[67] L. Danon, A. Díaz-Guilera, J. Duch, and A. Arenas, Journal of Statistical Mechanics: Theory and Experiment **2005**, P09008 (2005).

[68] E. Ravasz and A.-L. Barabási, Phys. Rev. E **67**, 026112 (2003).

[69] S. Fortunato and M. Barthélemy, Proceedings of the National Academy of Sciences **104**, 36 (2007).

[70] D. Goldberg, ACM Comput. Surv. **23**, 5 (1991).

[71] Wikipedia, "Kahan summation algorithm," `http://en.wikipedia.org/wiki/Kahan_summation_algorithm`.

초 록

서로 영향을 주고 받는 많은 개체들로 이루어진 계가 집단적인 행동을 하는 경우가 자주 있다. 집단적인 행동의 대표적인 예로 바로 동기화를 들 수 있다. 매우 간단한 경우로 각 개체를 위상을 갖고 있는 진동자로 생각하자. 진동자마다 고유한 성질, 즉 고유 진동수를 갖고 있기 때문에 상호작용이 없을 때에는 위상이 서로 다르다. 이제 진동자들이 강하게 상호작용을 하면, 시간이 갈수록 진동자들은 점점 위상을 맞추어 가게 되고, 결국 거의 모든 진동자들이 평균 위상에 가까운 위상을 갖게 된다. 이를 위상 동기화가 일어났다고 한다.

결합된 진동자들의 위상 동기화를 모사하는 간단하면서도 대표적인 모형으로 구라모토 모형이 있다. 이미 지난 수 십년 간 구라모토 모형에 관한 많은 연구들이 활발히 진행되었으며, 그 덕분에 위상 동기화에 대한 흥미로운 연구 결과들도 많이 알려져 있다. 1장 도입부에서는 동기화와 구라모토 모형을 소개하고, 선행 연구들이 밝혀 낸 연구 결과들을 간략히 소개하였다.

이 학위 논문은 본인이 물리학 박사 과정 동안 연구한 동기화와 관련된 주제 두 가지를 다룬다. 첫 번째 연구는 구라모토 모형의 동적 축척 현상에 대한 연구다. 지금까지의 선행 연구들 대부분은 동기화를 보이는 계의 정상 상태에 초점을 맞추었으나, 우리는 계가 정상 상태에 들어가기 전 동적 상태에 있을 때에도 초점을 맞추었다. 그 결과 결합 상수가 임계점 근처일 때, 구라모토 모형의 질서도가 시간에 따라 멱함수 꼴로 변화하는 것을 발견하였고, 이에 맞는 동적 축적 함수를 제안하였다. 계의 크기를 변화시키면서 시간에 따른 질서도의 변화를 구하고 동적 축척 관계를 이용하면, 여러 크기의 계로 그린 그래프들이 하나로 겹쳐지는 것을 확인할 수 있다. 더 나아가서 여기에 사용된 동적 축척 지수들은 유한 크기 축척 이론에서 이미 알려진 정적 축척 지수로 설명될 수 있음을 보였다. 완전히 연결되어 있는 네트워크, n 차원 정

방형격자, 무작위로 연결된 네트워크, 그리고 축척 없는 네트워크에서 구라모토 모형의 질서도에 대한 동적 축척 관계를 확인하였다. 각 진동자의 고유 진동수들의 분포로는 정규분포를 사용하였는데, 고유 진동수들이 똑같이 이 분포를 따르더라도 어떻게 생성되었느냐에 따라 질서도의 시간적 변화 양상이 달라지는 것을 발견하였다. 2장에서는 동적 축척 관계를 해석하는 데 바탕이 되는 유한 크기 축척 이론에 대하여 다루고, 3장에서는 동적 축척 관계에 대하여 실었다.

결합 상수가 임계점 근처에서 동적 축척 관계가 존재한다는 사실 자체로도 의미가 있으나, 이것이 중요한 이유가 한 가지 더 있다. 진동자 수가 아주 많은 계에서 임계 결합 상수를 컴퓨터 수치 계산으로 찾으려면, 계산 시간이 오래 걸린다. 구라모토 모형이 기술하는 미분 방정식으로 $\mathrm{d}t$ 시간 후의 위상들을 한 번 계산하는 데 걸리는 시간은 최적화를 하더라도 계의 크기에 비례하여 증가하며, 현실적으로 $\mathrm{d}t$ 시간 후의 위상들을 구하는 작업을 무한히 반복할 수도 없다. 동적 축척 관계에 대한 지식이 있으면, 계가 정상 상태에 도달할 때까지 계산할 필요 없이 동적 상태에 있을 때의 질서도의 변화를 분석하여 임계 결합 상수를 구할 수 있으므로 계산 시간을 크게 줄일 수 있게 된다. 임계점 근처에서 질서도가 멱함수 법칙을 따르는 현상을 이용하여 상대적 오차가 천분의 일 보다 작을 정도로 임계 결합 상수를 구별해 낼 수 있었다.

두 번째 주제는 구라모토 모형을 클러스터링 문제에 응용한 연구로 4장에서 다루었다. 클러스터링은 복잡계 네트워크에서 모듈 구조를 찾는 문제인데, 구라모토 모형의 상호작용 함수에 링크 중앙성에 의존하는 새 항을 도입하여 클러스터링에 활용하였다. 이 항이 도입되면서 링크 중앙성의 크기에 따라 링크 양 끝에 위치한 진자 사이에 0에서 π까지의 위상차가 생기게 된다. 변형된 구라모토 모형을 모듈 구조를 갖는 복잡계 네트워크에 적용하면, 각각의 모듈 안에서는 위상 동기화가 일어나는 반면, 전체 네트워크는 계속

무질서한 상태에 남아있게 된다. 이 현상을 바탕으로 기존의 다른 클러스터링 방법들과 비교하여 상대적으로 계산 시간은 적으면서도 정확도는 비슷한 새로운 클러스터링 알고리즘을 제안하였다.

마지막 5장에서 본 학위 논문 내용을 요약하고, 결론을 내리고 마무리하였다. 부록에는 구라모토 모형을 직접 수치 계산하는 데 있어서 도움이 될 만한 정보 몇 가지를 실었다.

주요어 : 동기화, 구라모토 모델, 상전이, 임계현상, 위상 동기화, 동적 축척, 관성 있는 구라모토 모델, 이력현상, 결합된 진동자, 비선형 동역학, 복잡계 네크워크, 유한 축척 이론, 클러스터링, 모듈 구조

학번 : 2006-22912